University of Amsterdam

Laboratoire Kastler Brossel
École Normale Supérieur

Master Thesis in Physics

Towards Critical Rotation

of an atomic Bose gas

Author:
Benno S. REM

Supervisors:
Dr. Kenneth J. GÜNTER
Prof. Dr. Jean DALIBARD
Dr. Robert SPREEUW

August 19, 2010

Abstract

This thesis provides a theoretical basis for shaping and rotating cold Bose gases with a modulated Time-averaged Orbiting Potential (TOP) trap. Furthermore, it documents the results our group obtained by realising the shaping and rotating in a ^{87}Rb experiment.

Our theoretical considerations are based upon a quadrupole field superimposed by a rotating bias field - the TOP trap. By changing the speed of rotation during a cycle, it is shown that the average single particle potential can be shaped as an arbitrary multipod. Modulation of the rotation speed is done by phase modulation of the currents flowing through the bias field coils. Using this concept made it possible to obtain the average potential of the multipod up to 4^{th}-order in spatial coordinates. Experiments confirmed the different trapping effects on the atoms for different symmetries - different shapes of the potentials - while changing the strength of the shaping (anisotropy strength).

Finally, these differently shaped potentials are set into rotation. Our group has investigated the influence of rotation on the number of atoms in the trap and the theoretical predictions done in this thesis turned out to be correct: the potential with a 2-fold symmetry (*Dipod*) is not trapping at critical rotation, whereas the potential with 4-fold symmetry (*Quadpod*) is. Hereby, critical rotation is defined as the rotation frequency at which the harmonic term of the potential is fully compensated by the centrifugal force. Measurements of the number of atoms at this frequency for different anisotropy strengths were done and compared with theoretical predictions. It turned out that the point at which all atoms are lost, due to the trap opening up, could be well predicted.

Contents

CONTENTS

Introduction

CHAPTER 1

Rotation

BOSE-EINSTEIN CONDENSATION - Ever since the *Cornell* and *Ketterle*-groups (Anderson, Ensher, Matthews, Wieman, & Cornell, 1995; Davis et al., 1995) in 1995 produced the first Bose-Einstein condensates (BEC) researchers have been interested in this phase of matter. The most stunning feature of a BEC is its phase coherence, which means that all the particles in the condensate have the same global phase and the cloud acts as if it is a single particle.

Another interesting feature is the behaviour of a condensate in a rotating system, because the Hamiltonian for a particle in a rotating field is equivalent to the Hamiltonian for a charged particle in a magnetic field. This mean that with rotating a condensate a system of charged particles in a strong magnetic field can be simulated (spin magnetism). Classically this similar behaviour is seen when comparing the *Coriolis* force to the magnetic *Lorentz* force.

When we want to look at the system of rotating a BEC the feature of phase coherence implies that the condensate has a velocity potential described by the phase of the condensate. Which means that if there are no singularities in the phase field the condensate can not have rotation. Feynman (Feynman, 1955) was the first to notice that in order to accommodate rotation the condensate needed to have singularities in its phase. With his path integral description of rotation in a condensate he could introduce these singularities and describe them. A singularity in the global phase is visible in a condensate as a point (tube) where the density of the condensate is zero. These points (tubes) are referred to as vortices.

1.1 Coriolis vs. Lorentz force

The *Coriolis* $\boldsymbol{F}_C$ and magnetic *Lorentz* $\boldsymbol{F}_L$ force are both conservative forces that arise for moving particles, given by

$$\boldsymbol{F}_C = -2m\boldsymbol{\Omega} \times \boldsymbol{v} \tag{1.1}$$
$$\boldsymbol{F}_L = -q\boldsymbol{B} \times \boldsymbol{v}, \tag{1.2}$$

where m is the mass of a particle in the co-rotating frame, $\boldsymbol{\Omega} = \Omega\,\hat{\boldsymbol{\Omega}}$ is the rotation vector with Ω the rotation frequency, q is the charge of a particle in a magnetic field $\boldsymbol{B}$ and $\boldsymbol{v}$ is the speed of either a charged particle in a magnetic field or a neutral particle in a rotational system.

From these equations it follows that the magnetic Lorentz force may be simulated by the Coriolis force when

$$\boldsymbol{\Omega} = \frac{q}{2m}\boldsymbol{B} = \frac{B}{2m}\hat{\boldsymbol{z}},$$

where we have taken $q = 1$ to simplify the equation, and B is the magnitude of the magnetic field. The rotation vector and magnetic field direction are chosen to be in the z-direction, which can be done without loss of generality.

1.2 Hamiltonian for a particle in a harmonic potential

A particle in a 2D Harmonic potential can be describe by the time-independent Schrödinger equation with the appropriate Hamiltonian (Landau & Lifshitz, 1977)

$$\boldsymbol{H}\,|\psi_n\rangle = E_n\,|\psi_n\rangle$$
$$\boldsymbol{H} = \frac{\boldsymbol{p}^2}{2m} + \frac{m\omega_\perp^2\boldsymbol{r}^2}{2}, \tag{1.3}$$

where $\boldsymbol{p}$ is the momentum operator, m is the mass of the particle, $\omega_\perp$ is the harmonic angular frequency in the xy-plane, and $\boldsymbol{r}$ the distance from the centre of the trap. The energy spectrum of the Schrödinger equation for a 2D harmonic oscillator is given by

$$E_n = \hbar\omega_\perp\,(n+1)\,, \tag{1.4}$$

where $n = n_x + n_y$ and $n_x, n_y \in \mathbb{N}$ are the quantum numbers of the excitation energy in their respective direction.

Going to the rotating frame requires an extra term to be added:

$$\begin{aligned}\boldsymbol{H} &= \frac{\boldsymbol{p}^2}{2m} + \frac{m\omega_\perp^2 \boldsymbol{r}^2}{2} - \Omega \boldsymbol{L}_z \\ &= \frac{(\boldsymbol{p} - \boldsymbol{A})^2}{2m} + \frac{1}{2} m \left(\omega_\perp^2 - \Omega^2\right) \boldsymbol{r}^2,\end{aligned}$$

where $\boldsymbol{L}_z$ is the angular momentum operator in the direction of the rotation vector. The energy spectrum of this system is given by

$$E(n, l_z, \Omega) = \hbar \left[\omega_\perp (n+1) - \Omega\, l_z\right],$$

where $\hbar\, l_z$ is the outcome of $\boldsymbol{L}_z$ working on $|\psi_n\rangle$ and corresponds to the projection of the angular momentum of $|\psi_n\rangle$ in the z-direction.

1.3 Critical Rotation and Lowest Landau Level

The limit $\omega_\perp = \Omega$ is referred to as the point of critical rotation. In that limit the energy spectrum of a particle in a rotating harmonic potential is given by

$$E_n(n, l_z) = \hbar\omega_\perp (n - l_z + 1) \tag{1.5}$$

and the possible values for l_z are limited by $-n \leqslant l_z \leqslant n$ and $n + l_z$ is even (Cohen-Tannoudji, Diu, & Laloë, 1977). This implies that the possible energy levels are given by $(2n_L + 1)\hbar\omega_\perp$ with $n_L \in \mathbb{N}$. All of these states n_L are infinitely degenerate, since all states $|k\, n, k\, l_z\rangle$ with $k \in \mathbb{N}$ ($2n_L = n - l_z$) have the same energy. These levels n_L correspond to the Landau levels that describe the energy levels of a charged particle in a magnetic field. The state of lowest energy ($n_L = 0$ and $n = l_z$) is called the lowest Landau Level (LLL) and is important for describing fractional Quantum Hall physics (Laughlin, 1999; Stormer, Tsui, & Gossard, 1999).

Figure 1.1 shows the energy spectrum of a 2D harmonic oscillator. In figure A the case for no rotation is shown and the energy spectrum of a 2D harmonic oscillator is shown. In figure B the critical rotation limit $\Omega \sim \omega_\perp$ is shown. Close to critical rotation the levels are not degenerate and the energy between the $l_z = 0$ and $l_z = k$ state is $k\,\hbar(\omega_\perp - \Omega)$. The energy difference between two following l_z states with same n_L is given by $\hbar(\omega_\perp - \Omega)$.

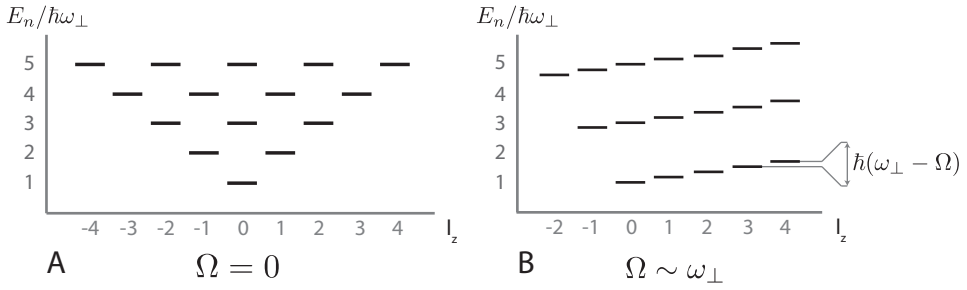

Figure 1.1: Figure A shows the situation without any rotation for a 2D harmonic oscillator ($\Omega = 0$). Figure B shows the case for rotation frequencies close to critical rotation ($\Omega \sim \omega_\perp$). At critical rotation $\Omega = \omega_\perp$ the levels with $n = l_z$ have the same energies and thus are infinite degenerate. These are called the *Landau levels*. The level with $n_L = 0$ is called the lowest Landau Level (LLL).

1.4 Vortices

So far everything was only on the level of single particle physics and the next step is to look at the wavefunction of a Bose-Einstein condensate (BEC) set into rotation. In order to do so a comparison between rotation in a classical fluid and in a quantum fluid is made.

1.4.1 Rotation of a classical fluid

The equilibrium velocity field in the lab frame of a rotating classical fluid is given by

$$\boldsymbol{v} = \boldsymbol{\Omega} \times \boldsymbol{r}, \tag{1.6}$$

where $\boldsymbol{v}$ is the velocity field at the position $\boldsymbol{r}$ and $\boldsymbol{\Omega}$ is the rotation vector. The curl of the velocity field,

$$\boldsymbol{\nabla} \times \boldsymbol{v} = 2\,\boldsymbol{\Omega}, \tag{1.7}$$

is called the "vorticity" of the flow.

1.4.2 Rotation of a quantum fluid

The many-body wavefunction of a Bose-Einstein condensate is given by (Pitaevskii & Stringari, 2003)

$$\Psi(\boldsymbol{r}) = \sqrt{n(\boldsymbol{r})}e^{i\theta(\boldsymbol{r})}, \tag{1.8}$$

where $n(\boldsymbol{r})$ is the density and $\theta(\boldsymbol{r})$ the phase of the wavefunction at position $\boldsymbol{r}$. This phase $\theta(\boldsymbol{r})$ is a global phase which means that all the atoms in the condensate have the same phase (phase coherence). In a place where the density is non zero, the velocity field of the condensate is given by (Landau & Liftshitz, 1977)

$$\boldsymbol{v} = \frac{\hbar}{m}\boldsymbol{\nabla}\theta(\boldsymbol{r}), \tag{1.9}$$

where m is the mass of a particle in the condensate and $\boldsymbol{\nabla}\theta(\boldsymbol{r})$ is the gradient of the phase. The vorticity of this field is given by

$$\boldsymbol{\nabla} \times \boldsymbol{v} = 0, \tag{1.10}$$

because the curl of a gradient is zero[1]. This seems to imply that it is forbidden for the condensate to have rotation. This problem of having no rotation was solved by Feynman (Feynman, 1955) who introduced the concept of singularities in the phase function. The singularities are shown in the density function as zero points (vortices). This solves the problem because with these singularities in the phase function it is possible to have rotation in the condensate and still have phase coherence.

1.4.3 Vortex filling factor

To characterise the rotation of a condensate, the circulation around the condensate is used

$$\oint_{\mathcal{C}} \boldsymbol{v} \cdot d\boldsymbol{l} = \frac{\hbar}{m}\oint_{\mathcal{C}} \boldsymbol{\nabla}\theta(\boldsymbol{r}) \cdot d\boldsymbol{l} = \frac{h}{m}N_v, \tag{1.11}$$

where N_v is the number of singularities (vortices) in the condensate. Following from the classical fluid the value for the coarse grained velocity is given by

$$\oint_{\mathcal{C}} \boldsymbol{v} \cdot d\boldsymbol{l} = \iint_S (\boldsymbol{\nabla} \times \boldsymbol{v}) \cdot d\boldsymbol{S} = \iint_{\mathcal{S}} 2\boldsymbol{\Omega} \cdot d\boldsymbol{S} = 2\,\Omega A, \tag{1.12}$$

[1] Care need be taken here, because this is only true for simply connected domains.

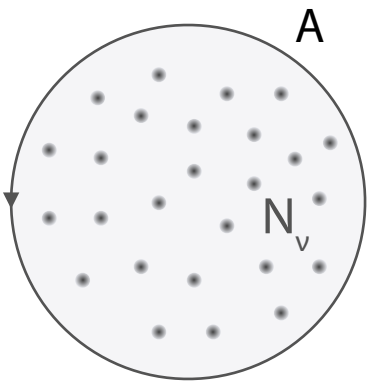

Figure 1.2: Graphical representation of a Bose-Einstein condensate with vortices in the condensate. There are N_v vortices in the cloud of area A.

where Stokes' theorem is used to introduce the curl of $\boldsymbol{v}$ and $\mathcal{S}$ is the integration range which has area A and surface element vector $d\boldsymbol{S}$. Although the classical velocity and the quantum velocity are clearly not the same, the contour integration in the limit of a large contour should recover similar result. This is similar to the correspondence principle, which states that in the limit of large quantum numbers the classical result should be obtained. Finally, the number of vortices N_v can be calculated by

$$N_v = \frac{2m\Omega}{h} A. \tag{1.13}$$

Closely related to this is the vortex filling fraction ν, which is defined as the number of atoms per vortex

$$\nu = \frac{N}{N_v} = \frac{N}{A} \frac{h}{2m\Omega}, \tag{1.14}$$

where N is the number of atoms.

The vortex filling fraction is a parameter to indicate in which rotation regime the system is. In figure 1.3 images of different regimes for ν are shown and the most interesting regime is where $\nu \leq 10$, which is the regime of strongly correlated states. The interesting features in this regime are that the vortex lattice will melt at $\nu \sim 10$ (Cooper, Wilkin, & Gunn, 2001) and at the point $\nu \sim 1$ strongly correlated states are produced that are related to the fractional Quantum Hall effect (Laughlin for $\nu = 1/2$, Pfaffian for $\nu = 1$). The group of *Chu* has announced to have reached this regime (Gemelke et al., 2010), but so far there are no images to complete the figure.

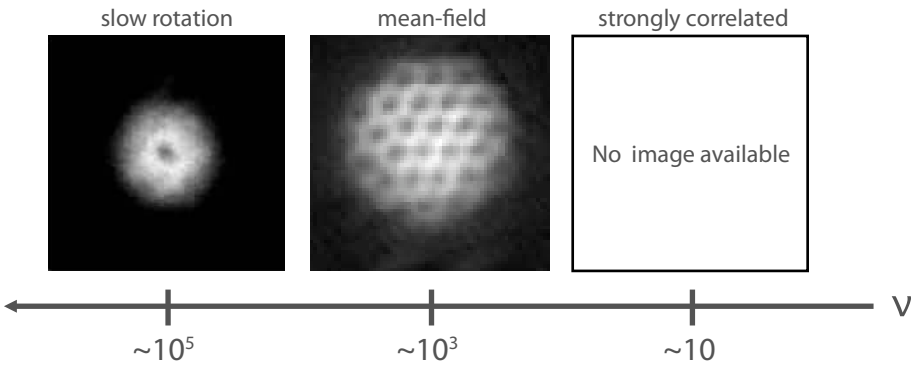

Figure 1.3: Shown are three regimes for ν the most left image is for slow rotation (can also be described by mean-field theory) and large ν which means many atoms per vortex (in the shown only one vortex on $\sim 10^5$ atoms). The middle image is in the mean field regime $\nu \sim 10^3$ and has a lot of vortices. This regime can still be described with mean field theory. The right image should show the strongly correlated regime $\nu \leq 10$, which has been reached (Gemelke et al., 2010), but there are no similar images so far. This regime would - in mean field theory - correspond to a few atoms per vortex, but the term vortices is not applicable, because in this regime, mean field theory is not valid anymore.The figures shown are taken from previous experiments at ENS.

1.5 Potential stability

When rotating a 2D harmonic anisotropy, due to the anisotropy a window of dynamical instability around critical rotation opens up (Guery-Odelin, 2000). To show that, a 2D harmonic anisotropic single particle potential - Dipod - is placed inside of the rotating frame,

$$U(\boldsymbol{r}) = \frac{1}{2}m\omega_\perp^2\left(x^2+y^2\right) + \frac{\epsilon}{2}m\omega_\perp^2\left(x^2-y^2\right) - \frac{1}{2}m\Omega^2\left(x^2+y^2\right), \quad (1.15)$$

with m the mass of the particle, $\omega_\perp$ the harmonic trapping frequency, Ω the rotation frequency of the system, ϵ the anisotropy strength and x, y the position variables. The equations of motion for this system are given by (Rosenbusch et al., 2002)

$$\ddot{x} - 2\Omega\,\dot{y} + \left(\omega_\perp^2\left(1+\epsilon\right) - \Omega^2\right)x = 0 \quad (1.16)$$

$$\ddot{y} + 2\Omega\,\dot{x} + \left(\omega_\perp^2\left(1-\epsilon\right) - \Omega^2\right)x = 0. \quad (1.17)$$

From these equations one can deduce that the potential is dynamically unstable in the range $\Omega \in \left[\omega_\perp\sqrt{1-\epsilon}, \omega_\perp\sqrt{1+\epsilon}\right]$. Dynamical instability means that the potential becomes anti-trapping in one or more directions. In the case of the Dipod there are two directions that are opening up depending on which side of the critical rotation the Dipod is rotating. This makes the anisotropic harmonic potential an unsuitable candidate for rotating close to critical rotation. With a higher-order potential it should be possible to keep the atoms stabilised up to critical rotation.

A first try to solve this problem was done by taking a potential of the next higher order - Tripod (Rath, 2010), where the potential is given by

$$U(\boldsymbol{r}) = \frac{1}{2}m\omega_\perp^2\left(\left(1-\alpha^2\right)\left(x^2+y^2\right) - \frac{\eta}{3}\left(3x^2y - y^3\right)\right). \tag{1.18}$$

Here the notation of (Rath, 2010) is used: $\alpha = \Omega/\omega_\perp$ and $\eta = 27\epsilon/8$. The potential has a region of stability within the dynamical unstable regime. This region has the shape of a triangle and can be characterised by three end points

$$r_2 = \frac{1-\alpha^2}{\eta}\hat{\boldsymbol{y}} \tag{1.19}$$

$$r_3 = \sqrt{3}\frac{1-\alpha^2}{2\eta}\hat{\boldsymbol{x}} - \frac{1-\alpha^2}{2\eta}\hat{\boldsymbol{y}} \tag{1.20}$$

$$r_4 = -\sqrt{3}\frac{1-\alpha^2}{2\eta}\hat{\boldsymbol{x}} - \frac{1-\alpha^2}{2\eta}\hat{\boldsymbol{y}}. \tag{1.21}$$

These points are equally spaced on a circle with radius

$$R = \frac{1-\alpha^2}{\eta}. \tag{1.22}$$

This shows that in the limit of critical rotation $\alpha \to 1$, the stable region vanishes and thus the potential is destabilised.

A solution for rotating at critical rotation exists in the form of a Quadpod which can be produced with phase modulation (see Chapters 6 for the shaping and 10 for rotating the shaped potential).

CHAPTER 2

Setup

THE experimental setup is in some detail discussed by Steffen Patrick Rath (Rath, 2010) in his thesis and to full extend in the PhD thesis of Marc Cheneau (Cheneau, 2009). The description given in this chapter is in principle a summary of both with some extra care on detail when describing the TOP trap, which is used to shape and rotate the potential.

The setup is mainly divided into two chambers: the first chamber "MOT chamber" to trap and pre cool atoms from a background gas and the second chamber "Science cell" which is used to further cool, obtain a condensate (or cold thermal cloud) and finally manipulate the cold atom cloud. In figure 2.1 these chambers are marked and it is shown that they are spatially separated and connected by a magnetic transport[1].

2.1 Sequence

Initially, ^{87}Rb atoms are captured from a background vapour in a Magneto-Optical Trap (MOT) (Raab, Prentiss, Cable, Chu, & Pritchard, 1987)[2]. Then the cloud is compressed by detuning the MOT laser beams (cMOT) (Townsend et al., 1995) and prepared for transporting by loading into a quadrupole trap. Next the cloud is magnetically transported (Greiner et al., 2001)[3] and loaded into a quadrupole trap in the 'Science cell'. In the quadrupole trap the evaporative cooling (Ketterle & Druten, 1996) is started and before the losses due to Majorana spinflips (Brink & Sukumar, 2006) become too large

[1] The magnetic transport is based on the Munich model (Greiner, Bloch, Hänsch, & Esslinger, 2001)

[2] This initial trapping stage lasts for $\sim 15\,s$ and captures $\sim 6 \cdot 10^9$ atoms

[3] The transport is done over 0.5 m and takes ~ 5 s during which $\sim 2.6 \cdot 10^9$ atoms are conserved.

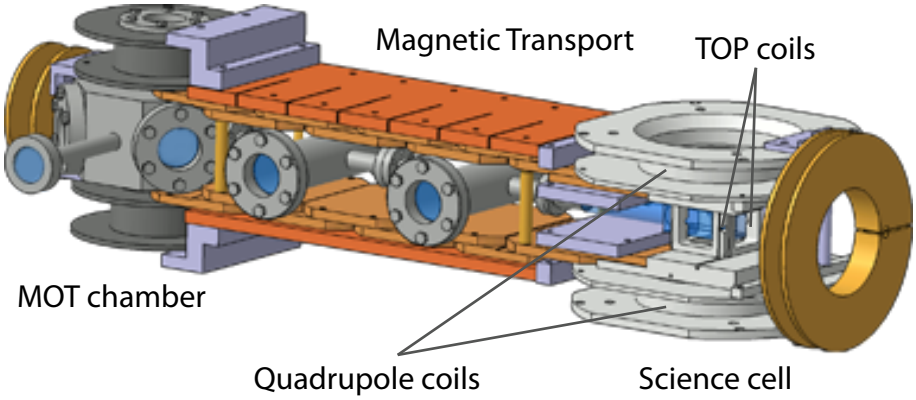

Figure 2.1: The ^{87}Rb setup used to do the experiments. The experiment is divided into two main chambers: The "MOT chamber", where the atoms are captured and pre-cooled from a background gas, and a "Science cell", where further cooling is done as well as the manipulation of the cloud. The two chambers are connected by a magnetic transport based on the Munich model (Greiner et al., 2001).

the cloud is transferred into a Time-averaged Orbiting Potential (TOP) trap (Anderson et al., 1995; Petrich, Anderson, Ensher, & Cornell, 1995), where the evaporative cooling (Rath, 2010) is continued until a Bose-Einstein condensate (BEC) is reached (Anderson et al., 1995; Davis et al., 1995)[4]. While the cloud is in the TOP trap, the gradient of the quadrupole field is lowered in order to decrease the mechanical stress on the coil holders, when rapidly turning off the magnetic trap. After the sequence, absorption imaging is used to characterise the cloud.

2.2 Time-averaged Orbiting Potential (TOP) trap

An extensive study of the TOP trap is given in Part I, but here we will list some experimental properties of the TOP trap used in our setup.

The TOP trap is based on a quadrupole trap with additionally a rotating homogeneous bias field, which lets the zero magnetic field point rotate

[4]The Bose-Einstein condensate contains $\sim 10^5$ atoms and is reached after ~ 50 s of evaporative cooling in the TOP trap.

around the cloud. The rotation frequency of our TOP bias field is on the order of $\omega_T = 2\pi \times 10\,\text{kHz}$, but since the domain of interest here is bounded - for large ω_T by the bandwidth of the amplifiers and for low ω_T by the micromotion in the trap - there is some interest in finding the right frequency[5]. The currents in the TOP coils are produced using two stereo audio amplifiers (Crest CPX 2600), one for each pair. The amplifiers have a bandwidth of $5\text{Hz} - 50\,\text{kHz}$.

2.2.1 Arbitrary waveform generator (Tabor WW1072)

For the input signals a programmable arbitrary waveform generator (Tabor WW1072, see figure 2.2) is used (Tabor Electronics, 2005). The signal generator can be programmed using GPIB and the device used in our experiment has an internal memory of 2 Mb per channel, which corresponds to 2 million waveform data points that can be stored per channel. The maximum sampling rate is $100\,\text{MS/s}$ and a single waveform needs to be defined by a multiple of 4 in the number of points with a minimum of 64. It is extremely important to not interrupt the sending of the data to the device, otherwise it may crash.

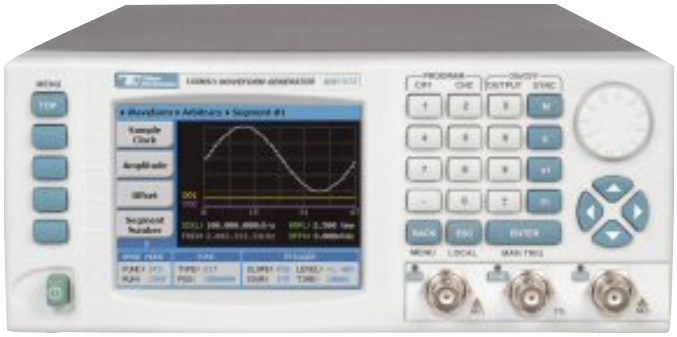

Figure 2.2: The Tabor WW1072 Arbitrary Waveform Generator. The generator has two outputting channels, used as input signals for the two TOP coils amplifiers. The device has the possibility to send waveform data points by GPIB and wait for a digital trigger.

Initially the Arbitrary waveform mode was used in **Gated** mode to generate the necessary signals for the TOP trap. This had the disadvantage of only being able to send one waveform. To give an example we are only able

[5] We have investigated $2\pi \times 5\,\text{kHz}$ and $2\pi \times 20\,\text{kHz}$ to see if the evaporation can be done more efficiently. For more information about the choice of ω_T we refer to Part I.

to send one waveform lets take a *sine* and a *cosine* for each channel respectively, then when a digital trigger is send to the device it output the *sine* and *cosine*. When the digital trigger is taken stopped the outputting is stopped. To have a different signal afterwards new data has to be send to the device.

One could argue to send the data points for the whole TOP trap sequence, but since there are 32 to 64 data points per bias field cycle needed and the memory is limited to 2MB, this would limit us to a couple of seconds of TOP trap, which is insufficient for the desired experiments.

Since the procedure above limits us to using only one type of signal during a run of the experiment we were, in the largest part of this thesis, limited by just replacing the standard TOP by the specific (phase modulated) potential. This had the disadvantage of doing the evaporative cooling in these (rotating) shaped potentials and the decompression either during evaporation or afterwards which is not an ideal situation.

These problems were overcome by using the **Segmented** mode in **Continuous Run** mode which has the ability to make segments with different waveforms and repeat these independently. To given an example we first send data for a normal TOP trap with a *sine* and a *cosine* and then send another waveform with more specific properties to do the shaping we want. Then a digital trigger pulse is used start the first segment and when we want to change to the next we send another one.

This technique allowed use to do evaporation and decompression (during or after evaporation) in a standard TOP trap and then switch to the desired shaped potential. This mode was used for taking the rotation spectra in figure 10.1. The switching between different segments is done with a digital trigger and this in principle makes it possible to generate as many different (rotating) shapes of the TOP trap as the memory allows[6].

More information about the programming of the Tabor WW1072 can be found in Appendix C.

[6]While this thesis was written, the group tried to optimise the sequence, as there seemed to be some triggering issues; for this reason no further data could be taken before the writing of this thesis

Part I

Standard TOP trap

CHAPTER 3

TOP trap

QUADRUPOLE TRAP - A quadrupole trap is the simplest purely magnetic trap, but it has the disadvantage of a vanishing magnetic field at the centre. This zero point causes non-adiabatic Majorana spin flips (Brink & Sukumar, 2006) and thus atom losses. To overcome this problem *Petrich et al.* introduced the TOP (Time-averaged Orbiting Potential) trap (Petrich et al., 1995). It is created by adding a rapidly rotating homogeneous bias field, which is rotating around the axis defined by the centres of the quadrupole field coils (Minogin, Richmond, & Opat, 1998). This field places the zero magnetic field point on a circle outside of the cloud rather than having it in the centre. At the same time a confining harmonic averaged potential is experienced by the atoms, which is required for keeping them trapped. The use of this trap allowed the *Cornell-group* to create the first Bose-Einstein condensate (BEC) in a dilute atomic gas of rubidium atoms (Anderson et al., 1995). Afterwards, BECs were also created using a plug beam to 'plug' the centre (Davis et al., 1995), a static non-zero minimum magnetic Ioffe-Pritchard (IP) trap (Mewes et al., 1996), and finally in 2001 also with a purely optical crossed dipole trap (Barrett, Sauer, & Chapman, 2001). The choice of our group was to use the TOP trap because it provides good optical access and great flexibility. Moreover, we can use the rotating bias field and tune its parameters for shaping and rotating the potential.

3.1 Magnetic trapping

As mentioned above, the simplest purely magnetic trap is a quadrupole trap. The setup of this consists of two coils placed at exactly twice their radius d from one another with their centres aligned on the z-axis. The cur-

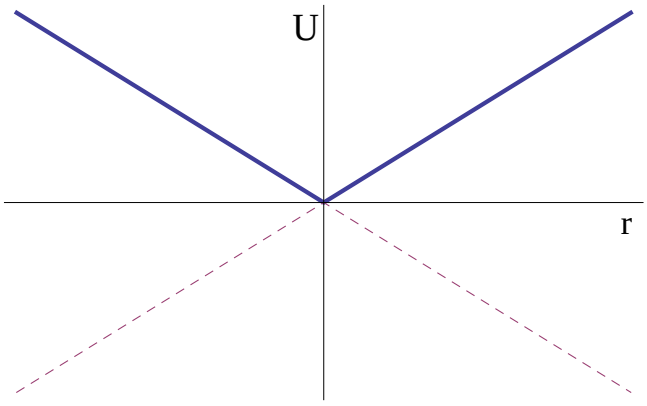

Figure 3.1: Potential of a quadrupole trap. The solid line shows the potential for atoms which have a negative projection of their magnetic moment on the axis of the magnetic field. At the centre the potential has a minimum and the atoms prefer to seek the lowest energy (low-field seekers). The dashed line shows the potential for atoms which have a positive projection of their magnetic moment in the direction of the magnetic field. They can lower their potential energy by leaving the trap, and thus are untrappable (high-field seekers). It is not possible to have a maximum in the magnetic field (Earnshaw's theorem), thus the high-field seekers can not be trapped with static magnetic fields.

rent flowing through each coil is equal, but oppositely circulating. This is called the *anti-Helmholtz* configuration.

The trap is based on the physical property that the magnetic moment $\boldsymbol{\mu}$ of an atom in a magnetic field $\boldsymbol{B}(\boldsymbol{r})$ at position $\boldsymbol{r}$ has the magnetic potential energy $U(\boldsymbol{r}) = -\boldsymbol{\mu} \cdot \boldsymbol{B}(\boldsymbol{r})$. This potential energy provides not only a *Larmor precession* of the magnetic moment $\boldsymbol{\mu}$ around the direction of the magnetic field $\boldsymbol{B}(\boldsymbol{r})$, but also a force that attracts atoms with a negative projection to a minimum in the magnetic field.

3.1.1 Larmor precession

The Larmor precession of a magnetic moment $\boldsymbol{\mu}$ around the direction of the magnetic field $\boldsymbol{B}(\boldsymbol{r})$ is characterised by the *Larmor frequency*

$$\omega_L = \left| \frac{\boldsymbol{\mu} \cdot \boldsymbol{B}(\boldsymbol{r})}{\hbar} \right|, \tag{3.1}$$

which corresponds to the angular frequency associated with the potential energy. The system tries to align this precessing with the magnetic field, to lower the potential energy. The *Larmor frequency* provides the time scale for the aligning.

To calculate the *Larmor frequency*, the magnetic field at position $\boldsymbol{r}$ is needed. One can use the Biot-Savart law to calculate this in the limit of small distances from the centre of the trap. The calculation gives a relation for the magnetic field of a quadrupole trap $\boldsymbol{b}(\boldsymbol{r})$,

$$\boldsymbol{b}(\boldsymbol{r}) = b(x - x_i)\,\hat{\boldsymbol{x}} + b(y - y_i)\,\hat{\boldsymbol{y}} - 2b(z - z_i)\,\hat{\boldsymbol{z}}, \tag{3.2}$$

with b the gradient of the magnetic field and $\boldsymbol{r_i} = (x_i, y_i, z_i)$ the centre of the trap. This approximation is only valid in the limit $|\boldsymbol{r} - \boldsymbol{r_i}| \ll d$, where d stands, either for the radius of the coils, or for the distance from the trap centre to the centre of each coil.

At the point $\boldsymbol{r} = \boldsymbol{r_i}$ the magnetic field vanishes, which causes the adiabatic approximation to be non-valid. Since there is a vanishing *Larmor frequency*, which triggers non-adiabatic Majorana spin flips that flip the magnetic moment of the atoms to an, in general, untrappable state and induces losses from the trap. Initially at high temperatures these losses are relatively small, because the relative density in the centre of the trap is low. On the contrary, at low temperatures the density at the trap centre is relatively high and the loss rate increases. This forced researchers to introduce other trap configurations. One possibility is to introduce a 'fast' rotating bias field which moves the zero point out of the cloud (Petrich et al., 1995).

3.1.2 Force due to spatial inhomogeneous magnetic field

The force on the atoms due to the spatial inhomogeneity of the magnetic field may be calculated using the gradient of the potential by

$$\boldsymbol{F}(\boldsymbol{r}) = -\boldsymbol{\nabla} U(\boldsymbol{r}) = -\mu \boldsymbol{\nabla} b(\boldsymbol{r}),$$

where μ is one of the possible negative projections of the magnetic moment in the direction of the magnetic field and $b(\boldsymbol{r})$ the magnitude of the magnetic field at position $\boldsymbol{r}$. The calculation can be simplified by taking the trap centre being $\boldsymbol{r_i} = (0, 0, 0)$. It follows that the force on a particle with magnetic moment μ equals to

$$\boldsymbol{F}(\boldsymbol{r}) = -\mu\, b\, \boldsymbol{\nabla} \left(\sqrt{x^2 + y^2 + 4z^2} \right) = -\mu\, b\, \frac{\bar{\boldsymbol{r}}}{\sqrt{x^2 + y^2 + 4z^2}}, \tag{3.3}$$

where $\bar{\boldsymbol{r}} = x\,\hat{\boldsymbol{x}} + y\,\hat{\boldsymbol{y}} + 4z\,\hat{\boldsymbol{z}}$ is similar to position vector $\boldsymbol{r}$ but with a rescaled z-axis. In the xy-plane the force turns out to be constant and pointing towards the centre, except for the point $\bar{r} = 0$, which is a singular point.

3.2 Rotating bias field

To remove the zero magnetic field point from the centre of the cloud a rotating bias field is added in the xy-plane (Minogin et al., 1998). This rotating bias field is given by

$$\boldsymbol{B}(t) = -B_0\Big[\cos(\Phi(t))\,\hat{\boldsymbol{x}} + \sin(\Phi(t))\,\hat{\boldsymbol{y}}\Big], \tag{3.4}$$

with B_0 the magnitude of the rotating bias field and $\Phi(t)$ is the phase function, which for a standard TOP trap is given by $\Phi(t) = \omega_T t$ where ω_T is the angular frequency.

A rotating homogeneous bias field displaces the zero magnetic field point out of the cloud and lets it rotate at a radius r_0 which is called the "radius of death". Figure 3.2 shows the displacement of a quadrupole magnetic field projection due to a bias field in the co-rotating frame. From the figure it can be seen that the zero magnetic field point is actually shifted in the direction opposite to the direction of the bias field. Using this makes it possible to define the "radius of death" r_0[1]:

$$r_0 = \frac{B_0}{b}. \tag{3.5}$$

The total magnetic field is simply recovered by adding the bias field to the quadrupole field (for simplicity we take the centre of the initial static trap to be at the centre of the coordinate system $r_i = 0$),

$$\boldsymbol{B}_T(\tilde{\boldsymbol{r}}, \Phi(\tilde{t})) = B_0\Big[\big(\tilde{x} - \cos(\Phi(\tilde{t}))\big)\,\hat{\boldsymbol{x}} + \big(\tilde{y} - \sin(\Phi(\tilde{t}))\big)\,\hat{\boldsymbol{y}} - 2\tilde{z}\,\hat{\boldsymbol{z}}\Big], \tag{3.6}$$

where we have introduced the phase function $\Phi(\tilde{t}) = 2\pi\tilde{t}$, which is used to define the phase of the rotating bias field during one cycle. The dimensionless variables $\tilde{\boldsymbol{r}} = \boldsymbol{r}/r_0$ is the position vector defined in units of the "radius of death", and $\tilde{t} = \omega_T t/2\pi$ a time variable normalised to one rotation cycle.

The magnitude of the total magnetic field $B_T(\tilde{\boldsymbol{r}}, \Phi(\tilde{t}))$ is given by

$$B_T(\tilde{\boldsymbol{r}}, \Phi(\tilde{t})) = B_0\sqrt{1 + \tilde{x}^2 + \tilde{y}^2 + 4\tilde{z}^2 - 2\left(\tilde{x}\cos(\Phi(\tilde{t})) + \tilde{y}\sin(\Phi(\tilde{t}))\right)}. \tag{3.7}$$

[1]The experiment described in this thesis has a "radius of death" that is on the order of $\simeq 1$ mm

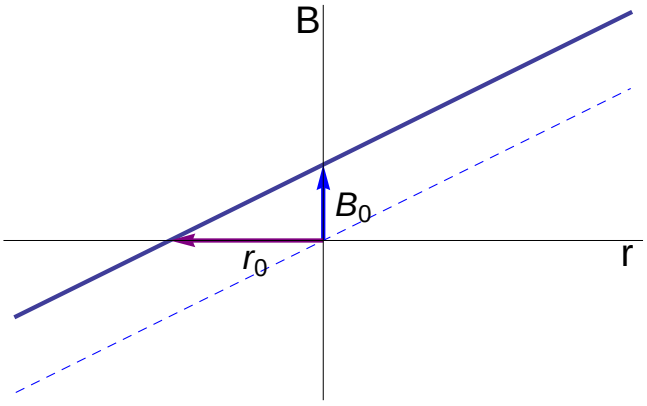

Figure 3.2: The magnetic field of the quadrupole field in the rotating frame of the bias field. The magnetic field is shifted by the bias field. The dashed blue line is the original quadrupole field without bias field and the thick solid line is the quadrupole field with the bias field. B_0 is the magnitude of the spatial homogeneous bias field and r_0 is the displacement of the zero magnetic field point (the "radius of death").

3.3 Time-averaged potential

Since the potential is rapidly rotating in time, some important limits to the rotation frequency of the bias field are apparent. The first requirement is that at all times the magnetic moments of the atoms need to be able to follow the rotation of the magnetic field. This limit can be characterised by the *Larmor frequency* (a theoretical investigation of the adiabatic approximation is done by (Franzosi, Zambon, & Arimondo, 2004)), associated to the rotating bias field:

$$\begin{aligned} \omega_L &= -\frac{\boldsymbol{\mu} \cdot \boldsymbol{B}(\boldsymbol{r}, t)}{\hbar}; \\ \omega_T &\ll \omega_L. \end{aligned} \tag{3.8}$$

Equation (3.8) gives the requirement for the adiabatic approximation to be valid and gives an upper limit to the rotation frequency (in our experiment[2] the Larmor frequency is of order $2\pi \times 5\,\mathrm{MHz}$).

On the other end, there is a lower limit which states that the movement of the zero magnetic field point is much faster then the Centre-Of-Mass

[2]The experiments are done with ^{87}Rb in the states $|F = 1, m_F = -1\rangle$ and $|F = 2, m_F = +1, +2\rangle$ (Rath, 2010) with Landé factors $g_1 = 1/2$ and $g_2 = -1/2$

(COM) motion, such that the cloud does not have the time to come close to the zero magnetic field point. This can be characterised by the harmonic trapping frequency $\omega_\perp$ of the averaged trap:

$$\omega_T \gg \omega_\perp, \tag{3.9}$$

where $\omega_\perp$ (which will be derived later on), in the experiments described by this thesis[3], is of the order of $2\pi \times 10\,\mathrm{Hz}$.

When these limits are valid, the average potential $U(\tilde{\boldsymbol{r}})$ can be calculated in the following way:

$$\begin{aligned} U_T(\tilde{\boldsymbol{r}}) &= \mu \int_0^1 B_T(\tilde{\boldsymbol{r}}, \tilde{t})\, d\tilde{t} \\ &= \mu B_0 \int_0^1 \sqrt{1 + \tilde{x}^2 + \tilde{y}^2 + 4\tilde{z}^2 - 2\left(\tilde{x}\cos(\Phi(\tilde{t})) + \tilde{y}\sin(\Phi(\tilde{t}))\right)}\, d\tilde{t}. \end{aligned} \tag{3.10}$$

This potential shows the importance of the limit in equation (3.8), because the integration is done over the magnitude of the magnetic field. An average over the magnetic field itself would again give rise to a quadrupole field, whereas now the magnetic moments $\boldsymbol{\mu}$ are able to follow and be aligned with the magnetic field $\boldsymbol{B}(\tilde{\boldsymbol{r}}, \tilde{t})$ at all times.

3.4 Expanding the potential in spatial coordinates

Expanding the integral in the potential of the magnetic field in equation (3.10) up to 4$^{\text{th}}$-order and integrating over time gives (Minogin et al., 1998)

$$U_T(\tilde{\boldsymbol{r}}) = \mu B_0 \left[1 + \frac{1}{4}\left(\tilde{r}^2 + 8\tilde{z}^2\right) + \frac{1}{64}\left(\tilde{r}^4 + 32\tilde{r}^2\tilde{z}^2 - 128\tilde{z}^4\right) + \mathcal{O}(\tilde{r}^6, \tilde{z}^6)\right]. \tag{3.11}$$

When looking in the plane of rotation (xy-plane $\tilde{z} = 0$), it is possible to compare the second order expansion with the equation of a harmonic oscillator,

$$\frac{\mu\, b^2}{4B_0} r^2 = \frac{1}{2} m\omega_\perp^2 r^2 \Rightarrow \omega_\perp = \sqrt{\frac{\mu\, b^2}{2mB_0}} \simeq 2\pi \times 10\,\mathrm{Hz}. \tag{3.12}$$

[3]The harmonic trapping frequency is measured using oscillation measurements

A similar comparison can be done for the 4^{th}-order terms,

$$\frac{1}{64}\frac{\mu\, b^2}{B_0} r^4 = \kappa r^4$$
$$\kappa = \frac{1}{64}\frac{\mu\, b^2}{B_0} > 0, \tag{3.13}$$

which implies that when the harmonic term is compensated by the centrifugal potential, the TOP-trap still has a quartic term which is trapping. Comparing this to the Ioffe-Pritchard trap, which has $\kappa < 0$, it is seen that in the TOP a natural trapping mechanism arises, whereas in the case of the Ioffe-Pritchard trap an additional anharmonic trap was needed (Bretin, Stock, Seurin, & Dalibard, 2004). If we compare these results with Appendix A it corresponds to the case $b = 0$ and $a > 0$ and thus trapping.

In figure 3.3 the exact potential of the TOP trap on the $\tilde{x}$ axis is shown. It is important to note, that at the centre a clear harmonic behaviour is visible at distances smaller then the "radius of death", whereas outside of the "radius of death", the trap becomes linear again, which is to be expected since the quadrupole trap is linear and the rotation outside the "radius of death" is just an addition of linear fields with the same slope, which is a linear potential itself.

3.5 Experiments using TOP trap to shape potentials

The *Oxford-group* have been using the TOP trap as basis for their research on rotating systems, but they modulated the trajectory of the zero magnetic field point to shape the averaged potential (Arlt et al., 1999). In contrast to the phase modulation used in our group. More about shaping (Part II) and rotation (Part III) in the rest of this thesis.

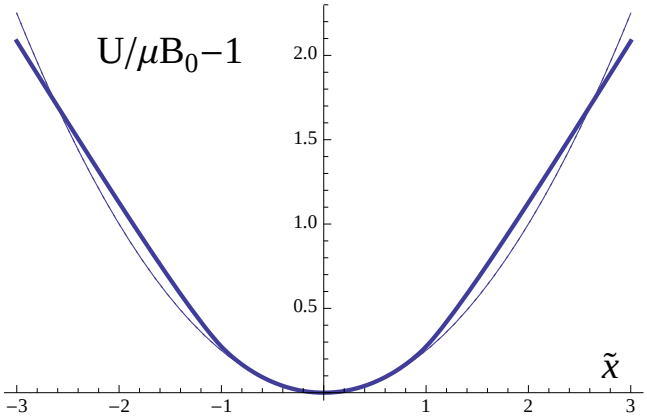

Figure 3.3: The thick blue line is the exact time averaged potential of the TOP trap. The vertical axis is in units of μB_0 and the horizontal axis shows for reasons of simplicity the radial x-axis of the trap in units of the "radius of death". The centre clearly shows at lowest order a harmonic trap, whereas outside of the "radius of death" there is no influence from the rotation and the trap again behaves like a standard quadrupole trap. The thin line is the potential approximated up to 2^{nd}-order. Within the "radius of death" the two have good overlapping, but outside a clear difference is shown.

CHAPTER 4

Discretisation

ROTATING field - The TOP trap uses a rapidly rotating bias field to make the zero magnetic field point cycle around the cloud (Minogin et al., 1998). In order to be able to rotate the cloud, it is necessary to introduce an anisotropy, which at a later stage can be rotated. The strongest n^{th}-order anisotropy can be created with just using n zero magnetic field points, which are distributed evenly over the cycle in space and time. For the TOP trap this would mean it starts in one point, stays there a certain period of time and then "jumps"[1] to the next point.

4.1 Zero magnetic field points

The formalism used in Chapter 3 is based on continuous variables. This means that the time resolution in principle is infinite, for practical reasons this is not feasible. The device[2] used to generate the signals that are sent to the amplifiers only accepts lists of data points. This required us to introduce a formalism for discrete rotation. The position of the zero magnetic field point can be described by the fast rotating spatial homogeneous bias field $\boldsymbol{B}(\Phi(\tilde{t}))$ (derived from equation 3.4) and the quadrupole field $\boldsymbol{b}(\boldsymbol{r})$,

$$\boldsymbol{r_0}(\Phi(\tilde{t})) = -\frac{\boldsymbol{B}(\Phi(\tilde{t}))}{b} = r_0\Big[\cos\big(\Phi(\tilde{t})\big)\,\hat{\boldsymbol{x}} + \sin\big(\Phi(\tilde{t})\big)\,\hat{\boldsymbol{y}}\Big]. \tag{4.1}$$

[1] Ideally this happens at infinite speeds, but in practice we are limited by the bandwidth of the signal amplifiers.

[2] The device we use for outputting the signals is an arbitrary waveform generator: Tabor WW1072.

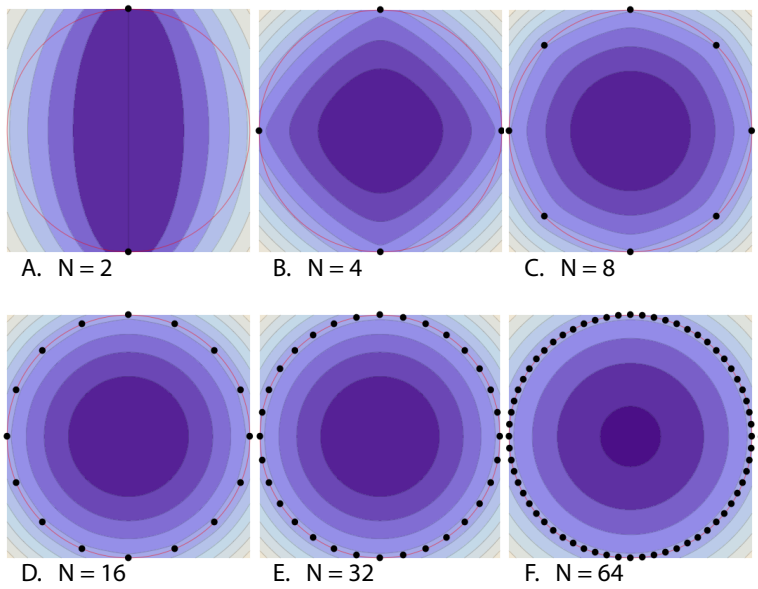

Figure 4.1: Potentials created by having η zero magnetic field points. From left to right and top to bottom the number of points per cycle is doubled in each following figure, starting with 2. *A*. clearly shows the strong Dipod potential; in *B*. a strong Quadpod potential is shown; in *C*. the 8^{th} order is still visible but already the harmonic term is taking over. Figures *D* through *F* are clearly approximating the round TOP trap. The red circle is at the "radius of death" and the black dots on the circle are the zero magnetic field points used to calculate the potential.

The first step is to discretise the phase function such that it only accepts integer numbers:

$$\Phi(\tilde{t}) = 2\pi\tilde{t} \rightarrow \Phi(i) = 2\pi\frac{i}{\eta}, \tag{4.2}$$

where $\eta \in \mathbb{N}$ is the number of zero points during one cycle and $i \in \{0, \ldots, \eta - 1\}$ is the discretised time iterator. However, there is a continuous current sent through the coils, thus finally, the potential produced is again continuous.

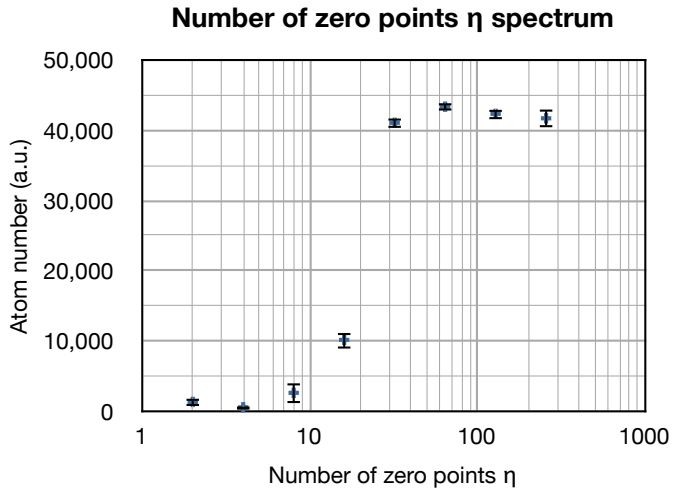

Figure 4.2: PRELIMINARY: Atom number vs. number of zero magnetic field points during one cycle η. The η data points are, from left to right: 2, 4, 8, 16, 32, 64, 128, 256, 512. There is a clear rise in the number of atoms from $\eta = 16$ to $\eta = 32$. The rest of this thesis will use $\eta = 64$ to have atoms. Shaping will be done with more dedicated phase modulation. The points in the graph are an average of multiple measurements and the error bars are the standard errors of each points, calculated by $\sigma_{\text{se}} = \sqrt{\langle y - \langle y \rangle \rangle^2}/N^2$, with N the number of points and $\langle y \rangle$ the average of y-values.

4.2 Discretisation anisotropy

Figure 4.1 shows a number of potentials with varying η. From this figure it is clearly shown that for $\eta \leq 8$, there is an anisotropy visible. For higher η the potential starts to look like a continuous standard TOP potential. Since the number of atoms in the trap drops below the point $\eta = 32$ the atoms do see the strong anisotropy. It needs to be noted that this drop is not well understood, since the potential of the trap does not seem to change significantly from $\eta = 16 \rightarrow 32$. At this stage, the only reasonable hypothesis we are able to formulate is that the change of direction of the bias field is too fast, such that the magnetic moment of the atoms does not follow. Further investigation could be done, by simulating the system keeping track of the

internal degrees of freedom (omitting the adiabatic approximation).

Conclusion and Summary

TOP TRAP - The TOP trap is produced by a quadrupole trap in addition to a rapidly rotating bias field. This causes the zero magnetic field point of the quadrupole to circle around the trap instead of staying fixed in the centre of the cloud.

This trap is an interesting tool for studying rotation, because it has a 4^{th}-order potential that is trapping. This means that when an atom cloud is set into rotation, near the point where the centrifugal force fully compensates for the harmonic trapping, the system will still be able to keep the cloud confined in the centre.

The 'static' TOP trap, however, does not have the ability to set the cloud into rotation. This requires us to introduce an anisotropy. Since discretisation of the TOP currents was needed for our equipment, the simplest way of creating the desired symmetry is by setting the number of zero points during one cycle equal to the desired anisotropy symmetry. We have done measurements on these types of anisotropic potentials and it turned out that there is a minimal number of points needed to be defined to have atoms in the trap.

It need be noted though that these experiments were done having an anisotropic TOP trap using the first mode described in section 2.2.1. This may cause effects that we are not able to explain and needs further investigation.

CHAPTER 4: DISCRETISATION

Part II

Static Anisotropic TOP trap

CHAPTER 5

Phase Modulation

STANDARD TOP traps do not have the ability to rotate a cloud, because they are shaped such that the zero magnetic field point has a round trajectory. Following symmetry arguments, the TOP trap potential is considered round when the trajectory is round[1] and the rotation speed of the zero magnetic field point is constant. There is a tool required for making the cloud rotate.

The *Oxford*-group (Arlt et al., 1999; Hodby, Hechenblaikner, Hopkins, Maragò, & Foot, 2001) chose to modulate the amplitude of the trajectory, thereby creating versatile elliptical potentials. The disadvantage using this method is that the "radius of death" depends on its angular position. This causes an oscillation of the "radius of death" and this may make it possible for the zero magnetic field point to enter into the cloud and cause losses. Our approach is to use phase modulation which holds the "radius of death" constant over one cycle.

Phase modulation is a method that is based on changing the rotation velocity of the zero magnetic field point. Since only the velocity is modulated, there is no change of the "radius of death". Phase modulation provides us with the tool for shaping and rotating the desired potential.

5.1 Formalism

In Chapters 3 and 4 the formalism based on (Minogin et al., 1998) is introduced. This is the basis of our concept of phase modulation of the TOP trap.

[1] There is always a 'static' anisotropy due to the not perfectly round trajectory of the zero magnetic field point.

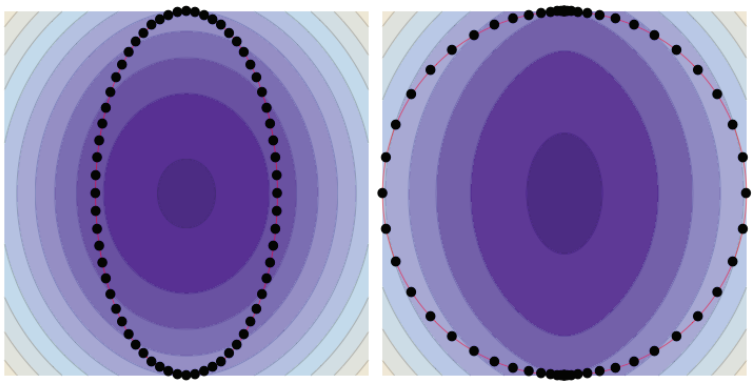

Figure 5.1: Figure A shows the potential for an amplitude modulated TOP trap which has the amplitude in the x-direction to be half the amplitude in the y-direction. The black dots are equally spaced points in time of the zero magnetic field point movement and the red circle is the radius of death. Figure B shows a similar situation but with phase modulation, where $\epsilon = 0.5$. Again the black dots are zero magnetic field points during one cycle equally spaced in time and the difference between the two plots is that in figure B there are two regions of grouped points and two regions of low point density. This is cased by the phase modulation. The contour plots have dark colours corresponding to low potential energies and light colours to high potential energies.

The zero magnetic field point is given in eq. (4.1),

$$\boldsymbol{r_0}(\Phi(\tilde{t})) = r_0\Big[\cos\left(\Phi(\tilde{t})\right)\hat{\boldsymbol{x}} + \sin\left(\Phi(\tilde{t})\right)\hat{\boldsymbol{y}}\Big],$$

where $\Phi(\tilde{t})$ was introduced to describe the phase of the rotating zero magnetic field point in units of one zero point cycle $\tilde{t}$. For a standard round TOP trap the phase function equals $\Phi(\tilde{t}) = 2\pi\tilde{t}$ and this can be used as the basis for the phase modulated phase function,

$$\Phi(\tilde{t}) = 2\pi\tilde{t} + \epsilon\sin(2\pi N\tilde{t}), \tag{5.1}$$

with ϵ the strength of the phase modulation (anisotropy) and N the order of the symmetry. To show what the *order of the symmetry* N is we calculate the rotational velocity and look at the speeding up and slowing down of the movement. The angular velocity of the zero point is given by the phase

velocity

$$\frac{d\Phi(\tilde{t})}{d\tilde{t}} = 2\pi + 2\pi N\epsilon\cos(2\pi N\tilde{t}). \tag{5.2}$$

The phase modulation changes the speed of the zero magnetic field point and creates N points where the zero point is maximally slowed down (the potential in this direction is relatively lower) and N points where the zero point is maximally accelerated (the potential in this direction is relatively higher). The velocity depends on the anisotropy strength and an interesting feature of the phase velocity is that for an anisotropy with $\epsilon > 1/N$, there are phases during a single cycle where the rotation of the zero point actually changes its direction.

5.2 Time-averaged potential

The rotation frequency is limited by the *Larmor frequency* (see eq. (3.8)), because it determines the validity of the adiabatic approximation. This means that the magnetic moments of the atoms need to be able to follow the magnetic field:

$$\omega_T(t) \ll \omega_L,$$

where we intentionally wrote $\omega_T(t)$ to emphasise the fact that the rotation frequency of the zero magnetic field depends on the phase modulation,

$$\omega_T(t) = \omega_{T,i} + \omega_{T,i}N\epsilon\cos(\omega_T N t), \tag{5.3}$$

with $\omega_{T,i}$ the initial rotation frequency of a standard TOP trap. This velocity is oscillating and the maximum value of this oscillation is given by

$$\omega_T^{\max} = \omega_{T,i}\left(1 + N\epsilon\right).$$

The new adiabatic approximation validity limit is given by

$$\omega_{T,i}\left(1 + N\epsilon\right) \ll \omega_L. \tag{5.4}$$

When this limit is fulfilled, it is possible to write the time-averaged potential of a phase modulated TOP trap (eq. (3.10)) as

$$U_T(\tilde{\boldsymbol{r}}) = \mu B_0 \int_0^1 \sqrt{1 + \tilde{x}^2 + \tilde{y}^2 + 4\tilde{z}^2 - 2\left(\tilde{x}\cos(\Phi(\tilde{t})) + \tilde{y}\sin(\Phi(\tilde{t}))\right)}\, d\tilde{t},$$

where we now use the phase function $\Phi(\tilde{t})$ from eq. (5.1).

5.3 Expanding the phase modulated potential

Solving the integral relation of the phase modulated potential is extremely difficult if not impossible to do, so first the potential was expanded in spatial coordinates and then integrate over one cycle. The expanded dimensionless potential ($\tilde{U}_T^{(n)}(\tilde{\boldsymbol{r}}) = U_T^{(n)}(\tilde{\boldsymbol{r}})/\mu B_0$ where n stands for the n^{th}-order expansion) is given by

$$
\begin{aligned}
\tilde{U}_T^{(0)}(\tilde{\boldsymbol{r}}) &= 1 \\
\tilde{U}_T^{(1)}(\tilde{\boldsymbol{r}}) &= \tilde{x}\, J_1(\epsilon)\delta_{N,1} \\
\tilde{U}_T^{(2)}(\tilde{\boldsymbol{r}}) &= \frac{1}{4}\Big[\left(\tilde{x}^2+\tilde{y}^2\right)\left(1+J_2(2\epsilon)\delta_{N,1}\right) \\
&\quad + \left(\tilde{x}^2-\tilde{y}^2\right) J_1(2\epsilon)\delta_{N,2} + 8\tilde{z}^2\Big] \\
\tilde{U}_T^{(3)}(\tilde{\boldsymbol{r}}) &= \frac{1}{8}\Big[-\tilde{x}^3 J_1(\epsilon)\delta_{N,1} \\
&\quad -\tilde{x}\tilde{y}^2 J_1(\epsilon)\delta_{N,1} \\
&\quad - 16\tilde{x}\tilde{z}^2 J_1(\epsilon)\delta_{N,1} \\
&\quad + \left(\tilde{x}^3 - 3\tilde{x}\tilde{y}^2\right)\left(J_3(3\epsilon)\delta_{N,1} + J_1(3\epsilon)\delta_{N,3}\right)\Big] \\
\tilde{U}_T^{(4)}(\tilde{\boldsymbol{r}}) &= \frac{1}{64}\Big[\left(\tilde{x}^4+\tilde{y}^4\right)\left(1-5\left(J_4(4\epsilon)\delta_{N,1} + J_2(2\epsilon)\delta_{N,2} - J_1(4\epsilon)\delta_{N,4}\right)\right) \\
&\quad + 4\left(\tilde{x}^4-\tilde{y}^4\right)\left(J_2(2\epsilon)\delta_{N,1} - J_1(2\epsilon)\delta_{N,2}\right) \\
&\quad + \tilde{x}^2\tilde{y}^2\left(2+30\left(J_4(4\epsilon)\delta_{N,1} + J_2(4\epsilon)\delta_{N,2} - J_1(4\epsilon)\delta_{N,4}\right)\right) \\
&\quad + \tilde{z}^2\left[32(\tilde{x}^2+\tilde{y}^2) + 96(\tilde{x}^2-\tilde{y}^2)\left(J_2(2\epsilon)\delta_{N,1} - J_1(2\epsilon)\delta_{N,2}\right)\right] - 128\tilde{z}^4\Big],
\end{aligned}
\tag{5.5}
$$

where $\delta_{N,p}$ with $p \in \mathbb{N}$ is the *Kronecker delta* used to indicate that it belongs to the p^{th} order of symmetry. $J_n(x)$ is the n^{th}-order Bessel function for x. These results are original in the sense that, this has not been done before and it can be applied more generally than the result from previous studies (Minogin et al., 1998). The result from these studies can even be retrieved by taking a special case ($N = 0$ and/or $\epsilon = 0$).

The standard TOP trap has the properties $\epsilon = 0$ and/or $N = 0$. Checking the potential using these parameters, we get

$$
U_T(\tilde{\boldsymbol{r}}) = \mu B_0 \left[1 + \frac{1}{4}\left(\tilde{r}^2 + 8\tilde{z}^2\right) + \frac{1}{64}\left(\tilde{r}^4 + 32\tilde{r}^2\tilde{z}^2 - 128\tilde{z}^4\right)\right],
$$

giving the same result for the standard TOP trap as eq. (5.5).

The case $N = 1$, in principle, off centres the cloud with respect to the "circle of death". This case might be interesting for studying clouds that are rapidly rotating around a circle. However, we have not done any further research on this topic.

The cases $N = 2, 3, 4$ will play a vital role in the coming parts of this thesis, because with these potentials we were able to create cloud that are rapidly rotating around their centre-of-mass. With the theoretical results obtained in this section we were able to explain some interesting phenomena appearing in our experiments.

CHAPTER 5: PHASE MODULATION

CHAPTER 6

Potential Shaping

SHAPING - The first efforts of shaping a TOP trap have been done by the *Oxford*-group (Arlt et al., 1999). They used amplitude modulation to produce an elliptical path for the zero magnetic field point. This again produces an elliptical time-averaged potential. This causes the "radius of death" to vary in time and possibly cut into the cloud. Our approach is to phase modulate the rotational movement. This allows use to make similar elliptical potentials using $N = 2$ - a (Dipod) - introduced in eq. (5.1), without changing the "radius of death". On the other hand, it gives us also a framework for producing higher order potentials.

6.1 Dipod

The Dipod potential is obtained by taking the *order of symmetry* parameter $N = 2$, thus retreiving

$$\Phi(\tilde{t}) = 2\pi\tilde{t} + \epsilon\sin(4\pi\tilde{t});$$

the averaged potential up to 2^{nd}-order in the xy-plane corresponding to that is given by

$$U_T(\tilde{\boldsymbol{r}}) = \mu B_0\left[1 + \frac{1}{4}\left(\tilde{x}^2\left(1 + J_1(2\epsilon)\right) + \tilde{y}^2\left(1 - J_1(2\epsilon)\right)\right)\right]. \tag{6.1}$$

To simplify the equation, one has to note that the Bessel function $J_1(2\epsilon)$ has only a limited range of values, which allows us to define a new variable $j \in [J_1^{\min}, J_1^{\max}]$ and replace the Bessel function $J_1(2\epsilon)$ by j, thus it follows

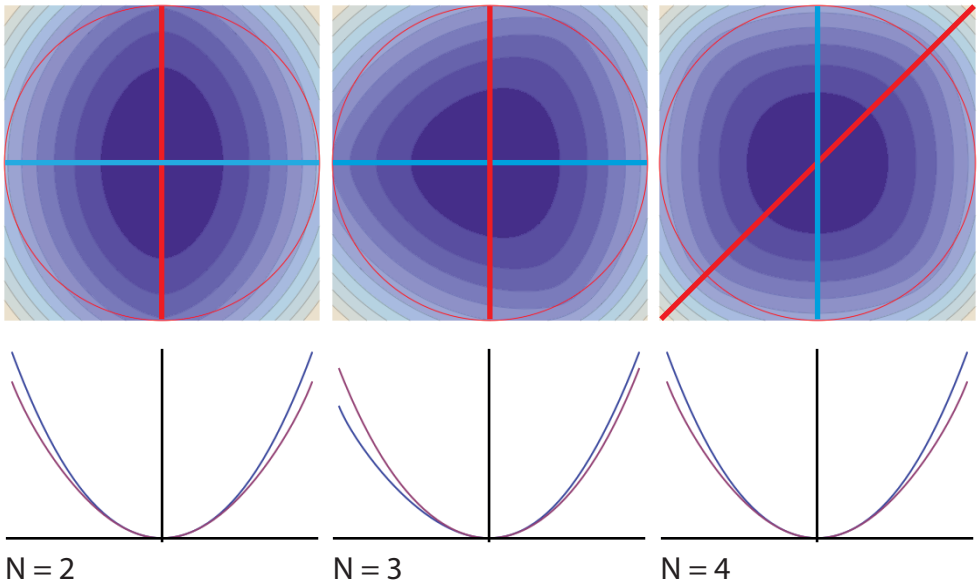

Figure 6.1: The order of symmetry N for the potential in the xy-plane. The red circle in the upper row of figures is the circle of death. From left to right are, respectively, shown the potentials for $N = 2$, $N = 3$ and $N = 4$ with an anisotropy $\epsilon = 0.5$. The figures in the upper row are contour plots of the potentials, where dark purple corresponds to lower energies and light purple to higher energies. The plotted lines show the axes of the figures in the lower row, where the colours of the lines in the upper plot correspond to the line colours in the lower plots. The potential for $N = 2$ has a Dipod shape and as can be seen from the cuts, the horizontal and vertical axes have different harmonic shapes (trapping frequencies). The case $N = 3$ - a Tripod - has a three fold symmetry and the horizontal cut shows the asymmetry, whereas the vertical one is symmetric. The case $N = 4$ - a Quadpod - shows the four fold symmetry and the vertical and diagonal cuts show the two main axes of the Quadpod. From these cuts it can be seen that the diagonal directions are less tightly confining than the vertical/horizontal direction.

for the potential that

$$U_T(\tilde{\boldsymbol{r}}) = \mu B_0 \left[1 + \frac{1}{4}\left(\tilde{x}^2\,(1+j) + \tilde{y}^2\,(1-j)\right)\right].$$

In figure 6.2, the Bessel function $J_1(k\epsilon)$ is given with the possible values of j given by the light blue area. The Dipod potential corresponds to the case $k = 2$.

The left hand graphics in Figure 6.1 show - in the upper row - a contour plot of the averaged potential, and - in the lower row - the cuts on the x-axis (blue line) and y-axis (red line). It is evident that the two cuts in the left column have different trapping frequencies. These trapping frequencies are given by

$$\omega_x = \omega_\perp \sqrt{1+j}; \tag{6.2}$$

$$\omega_y = \omega_\perp \sqrt{1-j}, \tag{6.3}$$

where ω_x (ω_y) is the trapping frequency in the x-direction (y-direction) and $\omega_\perp$ the trapping frequency in the xy-plane for the standard TOP trap.

Using these relations, we can define the anisotropy in terms of the trapping frequencies ω_x and ω_y:

$$j = \frac{\omega_x^2 - \omega_y^2}{\omega_x^2 + \omega_y^2}. \tag{6.4}$$

Since the Bessel function $J_1(2\epsilon)$ up to 1^{st}-order, in ϵ, is given by $j \simeq \epsilon$, these results correspond to the ϵ used by the *Oxford*-group (Arlt et al., 1999; Hodby et al., 2001). The range of anisotropies is obtained by taking the minimum and maximum of Bessel function $J_1(2\epsilon)$,

$$j \in \left[J_1^{\min}(2\epsilon), J_1^{\max}(2\epsilon)\right] = [-0.58, 0.58]\,. \tag{6.5}$$

6.2 Tripod

The Tripod potential is obtained by using $N = 3$ in eq. (5.5), up to 3^{rd}-order in the xy-plane, thus the potential becomes

$$U_T(\tilde{\boldsymbol{r}}) = \mu B_0 \left[1 + \frac{1}{4}\tilde{r}^2 + \frac{1}{8}\left(\tilde{x}^3 - 3\tilde{x}\tilde{y}^2\right) J_1(3\epsilon)\right].$$

The potential in the xy-plane is shown in the upper middle graph in figure 6.1. There a clear three fold symmetry is visible. The red and blue lines

show two directions of interest in the potential. In the lower middle graph, the line colours correspond to these special direction. The red line shows that on the y-axis the potential is symmetric, whereas the blue line shows the asymmetric behaviour in one of the Tripod's symmetry directions.

In figure 6.2 the general Bessel function $J_1(k\epsilon)$ is shown, for the 3^{rd}-order $k = 3$ needs to be used. Also for the Tripod the replacement $J_1(3\epsilon) \rightarrow j$ can be done, but care needs to be taken, because the ϵs corresponding to a values of j for the Tripod potential is different from the ϵs corresponding to the same j for the Dipod potential. Following from this replacement, is the potential

$$U_T(\tilde{\boldsymbol{r}}) = \mu B_0 \left[1 + \frac{1}{4}\tilde{r}^2 + \frac{1}{8}\left(\tilde{x}^3 - 3\tilde{x}\tilde{y}^2\right) j\right].$$

6.3 Quadpod

The Quadpod potential is obtained by using $N = 4$ in eq. (5.5), up to 4^{th}-order in the xy-plane, thus the potential becomes

$$U_T(\tilde{\boldsymbol{r}}) = \mu B_0 \left[1 + \frac{1}{4}\tilde{r}^2 + \frac{1}{64}\left(\left(\tilde{x}^4 + \tilde{y}^4\right)\left(1 + 5\,J_1(4\epsilon)\right) + \tilde{x}^2\tilde{y}^2\left(2 - 30\,J_1(4\epsilon)\right)\right)\right].$$

The right hand column in figure 6.1 in the first row a contourplot of the Quadpod potential $N = 4$ in the xy-plane. Again, the lines drawn in the contour plot are the directions of interest and symmetry. The red line shows that the potential in the direction $x = y$ is lower than in the other (blue line), which creates the rounded square shape.

The anisotropy can be described with only one parameter $J_1(4\epsilon)$. This means that it is possible to make groups of ϵ with $J_1(4\epsilon) = j \in [J_1^{\text{max}}, J_1^{\text{min}}]$, which is sufficient to define the anisotropy. Thus the replacement $J_1(4\epsilon) \rightarrow j$ can be made, but again care needs to be taken when the transformation back to ϵ is made. The replacement transforms the potential into the following form:

$$U_T(\tilde{\boldsymbol{r}}) = \mu B_0 \left[1 + \frac{1}{4}\tilde{r}^2 + \frac{1}{64}\left(\left(\tilde{x}^4 + \tilde{y}^4\right)\left(1 + 5\,j\right) + \tilde{x}^2\tilde{y}^2\left(2 - 30\,j\right)\right)\right].$$

The most remarkable feature following from this becomes apparent when $j = 0$ and $\epsilon = 0$ (the standard TOP trap), which has a potential that is perfectly symmetrical, but this is not only the case for $\epsilon = 0$. In fact, it is

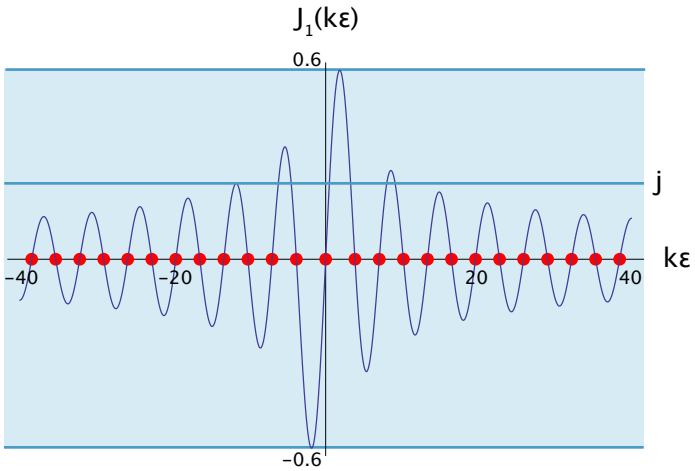

Figure 6.2: Shown is the Bessel function $J_1(k\epsilon)$ with being marked the zero crossing (red dots) and the range of values j (light blue area). At the zero crossings, there is special behaviour of the potentials at least up to the Quadpod, because their potentials $U_T(\tilde{\boldsymbol{r}})$ equal that of the standard TOP potential with $\epsilon = 0$.

true for all ϵ such that $j = 0$. The potential in the case of $j = 0$ is given by

$$U_T(\tilde{\boldsymbol{r}}) = \mu B_0 \left[1 + \frac{1}{4}\tilde{r}^2 + \frac{1}{64}\tilde{r}^4\right].$$

This is remarkable because, as can be seen from figure 6.2, there are a lot of zero crossings in the Bessel function $J_1(4\epsilon)$. From now on we will use the variable j to define the anisotropy.

CHAPTER 6: POTENTIAL SHAPING

CHAPTER 7

Anisotropy Strength

ANISOTROPY STRENGTH - the strength of the anisotropy is very important to investigate, because we are modulating the speed of the zero magnetic field point with phase modulation. This speed modulation may have a big influence on the atoms. For doing this we extend the formalism from Chapter 4 with the phase modulation phase function from Chapter 5.

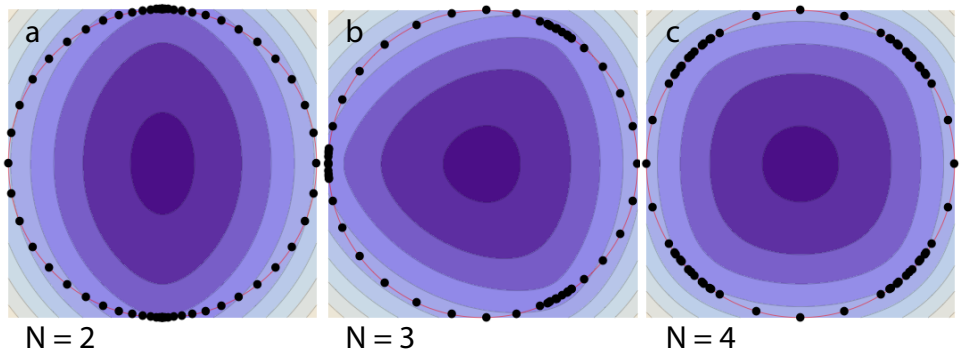

Figure 7.1: Shown are the discrete potentials for $N = 2$, $N = 3$ and $N = 4$. Each contour plot shows the zero magnetic field points spread out over the "circle of death" with the time in between the points being fixed. The number of points $\eta = 64$ and the anisotropy $\epsilon = 0.5$, which corresponds to $j \simeq 0.44$ for the Dipod, $j \simeq 0.55$ for the Tripod and $j \simeq 0.58$ for the Quadpod.

7.1 Discrete Phase Modulation

Recalling the phase modulation phase function from eq. (5.1) we can apply the discretisation transformation $\tilde{t} \to i/\eta$. This gives the discrete phase modulation phase function

$$\Phi(\tilde{t}) = 2\pi\frac{i}{\eta} + \epsilon \sin\left(2\pi N\frac{i}{\eta}\right), \tag{7.1}$$

where η is the number of time points per cycle. The potentials are shown for three values of N in figure 7.1. The black points show $\eta = 64$ points, where the period of time in between two points is constant.

7.2 Atom losses due to a static anisotropy

To see what the anisotropy strength does at the level of the atoms, we look at what happens to the number of atoms when changing the anisotropy strength ϵ while keeping the other parameters constant. In figure 7.2 the results of these measurements are plotted and an interesting feature is that the decrease in atom number in both the Dipod and Quadpod is linear in ϵ, whereas the Tripod seems to have a plateau first and then a sudden decrease in the atom number around $\epsilon = 0.25$.

A possible explanation for the decrease in atom number would be that the velocity of the zero magnetic field point is too high. This can be checked with eq. (5.2) and comparing the maximum value of this while changing N:

$$\left.\frac{d\Phi(\tilde{t})}{d\tilde{t}}\right|_{\text{max}} = 2\pi + 2\pi N\epsilon,$$

which for $N = 2$ and the point of total loss $\epsilon = 0.3$ gives $(d\Phi(\tilde{t})/d\tilde{t})_{\text{max}} = 1.2\,\pi$. For $N = 3$ and $\epsilon = 0.3$, it becomes $(d\Phi(\tilde{t})/d\tilde{t})_{\text{max}} = 0.9\,\pi$. Finally, for $N = 4$ and $\epsilon = 0.5$, we find $(d\Phi(\tilde{t})/d\tilde{t})_{\text{max}} = 2\,\pi$. These results, in principle, are connected to the results obtained in section 4.2. Since there are no clear indications for the loss of atoms, except for the change of velocity of the bias field that the atoms experience, it would be interesting to do simulations on the quantum motion of an atom. These simulations then would need to keep track of the atoms internal degree of freedom (no adiabatic approximation), and essentially simulate the evolution of two (for spin 1/2 particles) or three (for spin 1 particles) coupled time-dependent Schrödinger equations.

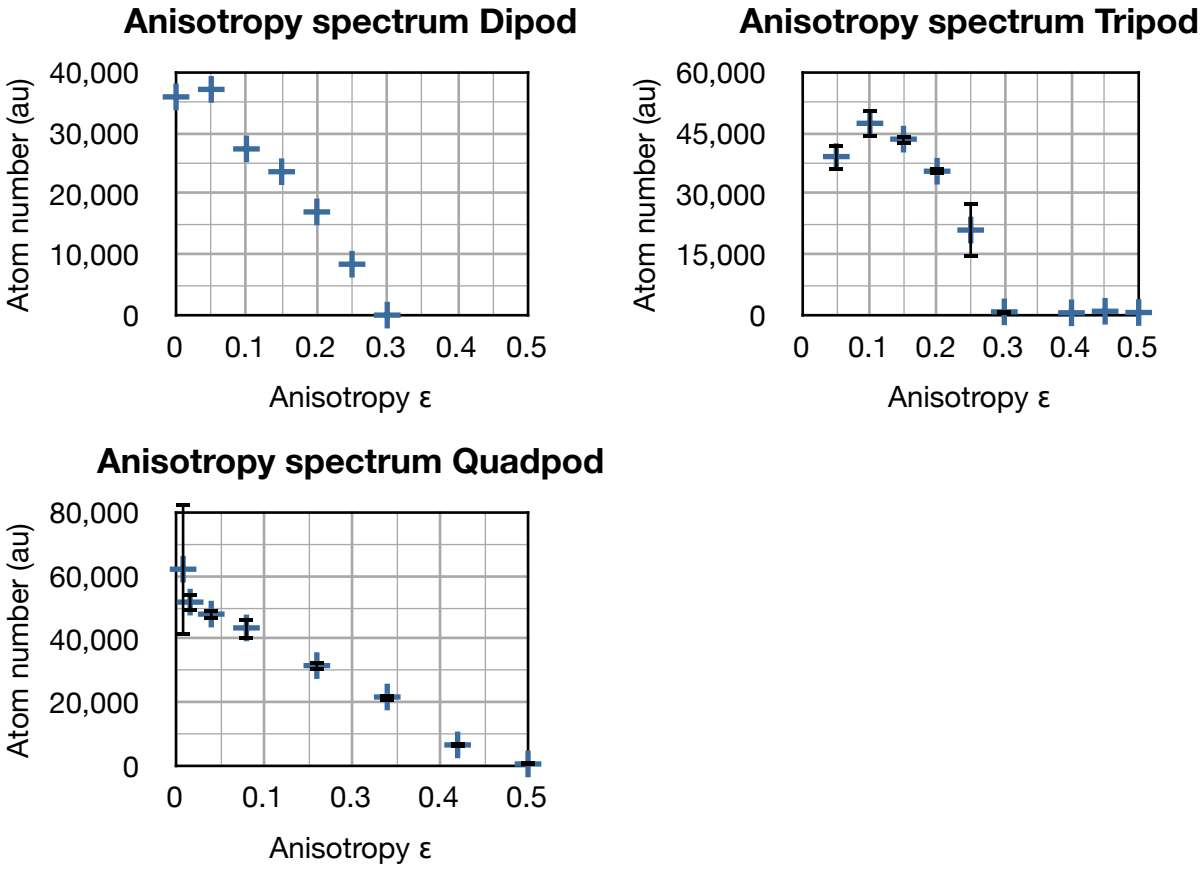

Figure 7.2: PRELIMINARY: Shown is the atom number as a function of the anisotropy ϵ in a static phase modulated TOP trap. Upper left is the Dipod $N = 2$ potential, upper right the Tripod potential $N = 3$ and finally lower left the Quadpod potential $N = 4$. The Dipod and Quadpod potentials show a linear relation in the decrease of atom numbers, whereas for the Tripod it looks more like a constant plateau and then a steep decrease. The points in the graph are an average of multiple measurements and the error bars are the standard errors of each points, calculated by $\sigma_{\text{se}} = \sqrt{\langle y - \langle y \rangle \rangle^2 / N^2}$, with N the number of points and $\langle y \rangle$ the average of y-values.

CHAPTER 7: ANISOTROPY STRENGTH

Conclusion and Summary

PHASE MODULATION - turned out to be an exhaustive tool for creating anisotropic traps with any desired symmetry. We have given a strong formalism, based on the formalism given in Part I, that describes the potential of the phase modulated TOP trap. This potential is really difficult to solve analytically, but expanding the magnitude of the magnetic field in spatial coordinates provided us with the necessary potential in the centre and allowed use to investigate some interesting potential symmetries. Three different symmetries have been characterised and discussed: the Dipod ($N = 2$), the Tripod ($N = 3$) and the Quadpod ($N = 4$).

Finally, the anisotropy of these potentials has been investigated by looking at the atom number as a function of the strength of the anisotropy. Both the Dipod and the Quadpod show linear decreasing behaviour until there are no atoms left. The Tripod on the other hand seems to have an plateau and then a threshold above which the atom number strongly decreases. These experiments showed some interesting, but unexplained behaviour that needs further investigation.

Also it need be noted that these experiments were done in the first run mode (discussed in subsection 2.2.1), which uses the phase modulated TOP trap during evaporation and decompressing of the TOP trap.

CHAPTER 7: ANISOTROPY STRENGTH

Part III

Rotating Anisotropic TOP trap

CHAPTER 8

Co-Rotating Frame

NATURAL ROTATION - The TOP trap has a natural rotation in the movement of the zero magnetic field point. The previous chapter used phase modulation to modulate this rotational movement and use it to shape the potential. The rotation can only be done in two dimensions and the plane of choice is the xy-plane, which makes the description of the phase modulation easier but not necessarily less general. The next step is to set the phase modulated shape into rotation.

The set a system into rotation - in the xy-plane - the rotation matrix

$$\boldsymbol{R}(\Omega t) = \begin{bmatrix} \cos\Omega t & -\sin\Omega t \\ \sin\Omega t & \cos\Omega t \end{bmatrix} \tag{8.1}$$

is used, where Ω is the angular rotation frequency of the rotating system.

8.1 Potential in co-rotating frame

The movement of the zero magnetic field point described by $\boldsymbol{r}_0$ is set into rotation by multiplying the equations of motion by the rotation matrix:

$$\begin{aligned} \boldsymbol{r}_{\mathbf{0}}^{\text{rot}}\left(\Phi(\tilde{t})\right) &= \boldsymbol{R}\left(\Omega t\right) \cdot \boldsymbol{r}_{\mathbf{0}}\left(\Phi(\tilde{t})\right) \\ &= \boldsymbol{r}_{\mathbf{0}}\left(\Phi(\tilde{t}) + \Omega t\right) = \boldsymbol{r}_{\mathbf{0}}\left(\Phi(\tilde{t}) + 2\pi\,\delta\,\tilde{t}\right), \end{aligned}$$

where we have introduced $\delta = \Omega/\omega_T$. If we then change the time variable to a dimensionless time in the rotating frame,

$$\tilde{t} = (1+\delta)\frac{\omega_T}{2\pi}t \tag{8.2}$$

and take the phase modulation function (eq. (5.1))

$$\Phi^{\text{rot}}(\tilde{t}) = 2\pi\tilde{t} + \epsilon\sin(2\pi N\tilde{t}) + 2\pi\,\delta\,\tilde{t}. \tag{8.3}$$

This means that when looking in the co-rotating frame the angular frequency of the rotating zero magnetic field point is reduced by a $\delta\omega_\perp$. Important then for the atoms is that in the rotating frame they still see a averaged potential (eq. (3.9)) with a reduced ω_T,

$$(1-\delta)\,\omega_T \gg \omega_\perp. \tag{8.4}$$

Since we are interested in the limit of critical rotation which means $\Omega \simeq \omega_\perp$, it follows that $\delta \simeq \omega_\perp/\omega_T \ll 1$, thus validating the limit in eq. (8.4). The potential in the rotating frame is then given by eq. (3.10) with a redefined dimensionless time $\tilde{t}$ given by eq. (8.2). Since the integration limits in this case stay defined over one integration period, the integral keeps having the same outcome. Only when the limit eq. (8.4) is violated the potential is not well defined in the co-rotating frame. The potential in the co-rotating frame is given by the potential in the lab frame (eq. (3.10)) with the phase modulation function $\Phi(\tilde{t})$ given by eq. (5.1):

$$U_T(\tilde{\boldsymbol{r}}) = \mu B_0 \int_0^1 \sqrt{1+\tilde{x}^2+\tilde{y}^2+4\tilde{z}^2-2\left(\tilde{x}\cos(\Phi(\tilde{t}))+\tilde{y}\sin(\Phi(\tilde{t}))\right)}\,d\tilde{t}.$$

CHAPTER 9

Discretising Rotation

DISCRETISING - The discretisation needs some special caution, because we need the periods of two rotations to be overlapping. The first arising for the 'fast' rotating bias field of the TOP and the second for the 'slow' rotation of the averaged potential. This restriction is implied by the equipment used, because our equipment takes a point list for one outputting period (T_{out}) and repeatedly outputs this after one another. This requires the periods of both the 'fast' and 'slow' rotation to be fully finished before starting a new period.

9.1 Discretisation formalism

The outputting period T_{out} is in general repeated and then it is important that there is no phase jump in between the end and the beginning of the period. This makes it important to define one outputting period as a multiple of both the 'short' rotation period ($T_{\text{TOP}} = 2\pi/\omega_T$) and the 'long' rotation period ($T_{\text{rot}} = 2\pi/\Omega$):

$$T_{\text{out}} = q\,T_{\text{TOP}} = p\,T_{\text{rot}}, \tag{9.1}$$

where $p, q \in \mathbb{N}$ are respectively the number of cycles of the zero point and the number of cycles of the rotating anisotropic potential. Then we can define a relation between the rotation frequencies by

$$\begin{aligned} q\,\frac{2\pi}{\omega_T} &= p\frac{2\pi}{\Omega} \\ \delta = \frac{\Omega}{\omega_T} &= \frac{p}{q} \in \mathbb{Q}^+. \end{aligned} \tag{9.2}$$

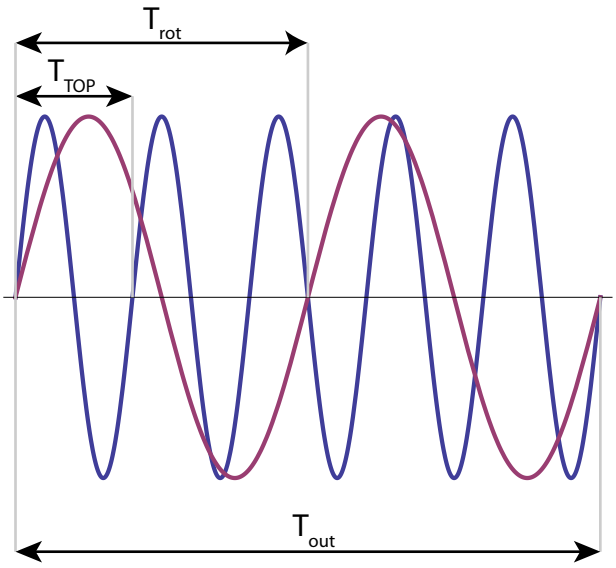

Figure 9.1: Shown are two sinusoidal function: the blue line corresponding to a 'fast' oscillation (T_{TOP}) and the red line to a 'slow' oscillation (T_{rot}) after one oscillation of the red line the blue line is not in the same phase. After the second oscillation of the red line both are in the same phase of the oscillation (T_{out}). These oscillations would correspond to $p = 2$ and $q = 5$ in eq. (9.1). Note: the number of oscillations is arbitrary and only used to show how the different cycle periods correspond need to overlap.

With this transformation we can define the discrete rotational phase modulation function (following eq. (8.3)) by

$$\Phi^{\text{rot}}(i) = 2\pi\frac{i}{\eta} + \epsilon\sin(2\pi N\frac{i}{\eta}) + 2\pi\,\frac{p}{q}\frac{i}{\eta}. \tag{9.3}$$

In principle, this function has all the necessary information to do the rotations, but since we are limited by memory, we need to refine our procedure. To do so two schemes need to be introduced for varying the rotation frequency Ω. A characterisation of the different schemes has to be based on the amount of memory it consumes, meaning the number of data points N_{out}:

$$N_{\text{out}} = \eta \cdot q. \tag{9.4}$$

The first scheme takes a fixed q and varies the p. The advantage of this scheme is the fixed frequency resolution. On the down side, to have a high

frequency resolution q needs to be on the order (or higher) of $\omega_T/2\pi$ which takes up a lot of memory and only corresponds to a resolution of $1\,\text{Hz}$, which will be explained in the following subsections. The second scheme uses a fixed p and changes the q which takes up less memory, but the frequency resolution and memory uses are not fixed anymore.

9.1.1 Fixed frequency resolution

When choosing the fixed frequency resolution option, it means that q is kept constant and p is varied to vary the rotation frequency

$$\Omega(p) = \frac{\omega_T}{q} p. \tag{9.5}$$

Then the change in frequency between two points is given by

$$\Delta\Omega = \frac{\omega_T}{q}\big((p+1) - p\big) = \frac{\omega_T}{q}. \tag{9.6}$$

On the downside, q needs to be larger than $\omega_T/2\pi \simeq 10\,\text{kHz}$ to get a resolution of $1\,\text{Hz}$ or better. Furthermore, an often used q is 20000, which gives a resolution of $0.5\,\text{Hz}$, and the number of points per cycle $\eta = 64$. The number of points that needs to be defined, for a full waveform, is given by

$$N_{\text{out}} \simeq 1.28 \cdot 10^6.$$

Since each point corresponds to one byte, this fills up more than half of the total memory per channel[1].

The important range for now is $p = 0$ (no rotation) to $p \simeq 100$ which corresponds to the range $0 - 50\,\text{Hz}$. Only a very small range of possible values $p \in \{0, \ldots, q\}$ is used so this scheme seems to work inefficient, but the definition is clear and simple to use.

9.1.2 Fixed period resolution

The other possible parameter to change Ω is q, while leaving p constant. The relation for Ω is then given by

$$\Omega(q) = \omega_T\, p\, \frac{1}{q} \tag{9.7}$$

[1]The Tabor WW1072 uses points that have a precision defined by one byte and in our case the device has a total of $2\,\text{MB}$ memory per channel.

and the frequency resolution following from this becomes:

$$\Delta\Omega = \omega_T \, p \left(\frac{1}{q} - \frac{1}{q+1} \right). \tag{9.8}$$

The resolution depends on $\big(1/q - 1/(q+1)\big)$, which decreases in case of an increasing q. As we are interested in the limit $\Omega \ll \omega_T$, this scheme is quite suitable. This can be shown when looking at the case $p = 1$. In this case one potential rotation cycle is defined; one rotation cycle is on the order of $100\,\text{ms}$, thus the total time T_{out} is $100\,\text{ms}$. Comparing this to the cycle time of the zero magnetic field point ($\simeq 0.1\,\text{ms}$),

$$\Delta\Omega = \omega_T \left(\frac{1}{q} - \frac{1}{q+1} \right).$$

It follows that for rotation frequencies Ω between $2\pi \times 1\,\text{Hz}$ and $2\pi \times 100\,\text{Hz}$ we only need the range $q \in \{100, \ldots, 1000\}$. This drastically reduces the number of points needed

$$N_{\text{out}}^{\text{max}} \simeq 6.4 \cdot 10^4$$

and the resolution range for these q's and $\omega_T \simeq 2\pi \times 10\,\text{kHz}$ is

$$\Delta\Omega \in 2\pi \times \left[\frac{10}{1001}, \frac{100}{101} \right] \text{Hz}.$$

Improving this resolution can be done by increasing both p and q. The only point that is not possible to reach in this scheme is no rotation but this is easily solved by taking $p = 0$.

This second scheme can be characterised as being period resolution fixed, because two consecutive q points give a cycle period resolution given by

$$\Delta T_{\text{rot}} = \frac{T_{\text{TOP}}}{p} \left((q+1) - q \right) = \frac{T_{\text{TOP}}}{p},$$

which is constant for all q.

CHAPTER 10

Results

RESULTS obtained with rotating phase modulated potentials will now be discussed. There are two main phenomena we have been studying that will be introduced in this part. The first phenomena is based on the effect of the rotation frequency Ω on the atoms and the second on the effect of a given the anisotropy ϵ on the atoms at critical rotation. The potential function in the rotating frame is given by eq. (3.10); the phase modulation function by eq. (5.1); in addition to that, the centrifugal potential is needed. The combined potential is given by

$$U_T(\tilde{\boldsymbol{r}}) = \mu B_0 \left[\int_0^1 \sqrt{1 + \tilde{x}^2 + \tilde{y}^2 + 4\tilde{z}^2 - 2\left(\tilde{x}\cos(\Phi(\tilde{t})) + \tilde{y}\sin(\Phi(\tilde{t}))\right)}\, d\tilde{t} - \frac{\alpha^2}{4}\tilde{r}^2 \right]$$

with

$$\Phi(\tilde{t}) = 2\pi\tilde{t} + \epsilon\sin(2\pi N\tilde{t}),$$

where $\alpha = \Omega/\omega_\perp$ is a measure of the critical rotation, since $\alpha = 1$ corresponds to the point of critical rotation.

10.1 Rotation Spectra

To investigate the influence of the rotation frequency Ω on the atoms we compare two cases: the Dipod $N = 2$ and the Quadpod $N = 4$. First for the Dipod, we can write down the expanded phase modulated potential (we have omitted the constant part, because it only shifts the potential energy up):

$$U_T(\tilde{\boldsymbol{r}}) = \mu B_0 \left[\frac{1-\alpha^2}{4}\tilde{r}^2 + \frac{j}{4}\left(\tilde{x}^2 - \tilde{y}^2\right) \right] \tag{10.1}$$

and secondly for the Quadpod:

$$U_T(\tilde{\boldsymbol{r}}) = \mu B_0 \left[\frac{1-\alpha^2}{4}\tilde{r}^2 + \frac{1}{64}\left(1+5j\right)\left(\tilde{x}^4+\tilde{y}^4\right) + \frac{1}{64}\left(2-30j\right)\tilde{x}^2\tilde{y}^2 \right]. \tag{10.2}$$

In figure 10.1 the rotation spectra for the Dipod (left) and Quadpod (right) are plotted. The measurements are done by fitting the atom number of a phase modulated rotating potential ($\epsilon = 0.03$, thus $j \simeq 0.03$ for a Dipod and $j \simeq 0.06$ for a Quadpod) and dividing it by a next run with a fit of the atom numbers in a standard TOP trap ($\epsilon = 0$, thus $j = 0$). This was done to filter out some longterm drifts.

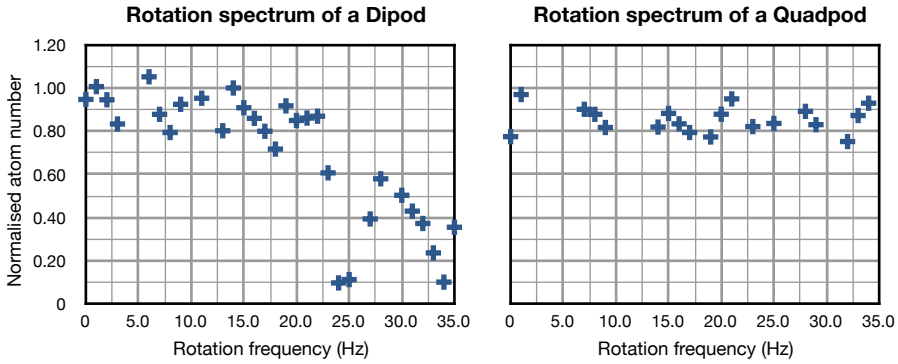

Figure 10.1: PRELIMINARY: The left picture shows the rotation spectrum for a Dipod ($N = 2$) potential. On the right the rotation spectrum for a Quadpod ($N = 4$) is shown. The normalised atom numbers are measured by doing first a run with a rotating TOP trap ($\epsilon = 0.03$, thus $j \simeq 0.03$ for a Dipod and $j \simeq 0.06$ for a Quadpod) and then doing another run without rotation ($\epsilon = 0$), fit the number of atoms of both runs and divide the first one by the second.

10.2 Anisotropy at Critical Rotation

To measure the strength of the anisotropy ϵ of an Quadpod potential at critical rotation we can take the potential defined in eq. (10.2) for the Quadpod and use the critical rotation criterium ($\alpha = 1$) and find

$$U_T(\tilde{\boldsymbol{t}}) = \frac{\mu B_0}{64}\left[(1+5j)\tilde{r}^4 + (2-30j)\,\tilde{x}^2\tilde{y}^2\right]. \tag{10.3}$$

In Appendix B the properties of a 4^{th}-order potential are explored and, using the following inequalities defined in eqs. (B.3) and (B.4),

$$a > 0;$$
$$b > -2a$$

to determine whether the 4^{th}-order potential is trapping at the centre. We can find limits for j such that the potential is trapping. In the case of the phase modulated 4^{th}-order potential $a = 1 - 5j$ and $b = 2 - 30j$. With these relations we can define a range for j:

$$j > -\frac{1}{5} \tag{10.4}$$
$$j < \frac{1}{5}. \tag{10.5}$$

In figure 10.2 these limits are plotted. The blue shaded areas are the trapping areas and the red areas are the anti-trapping areas.

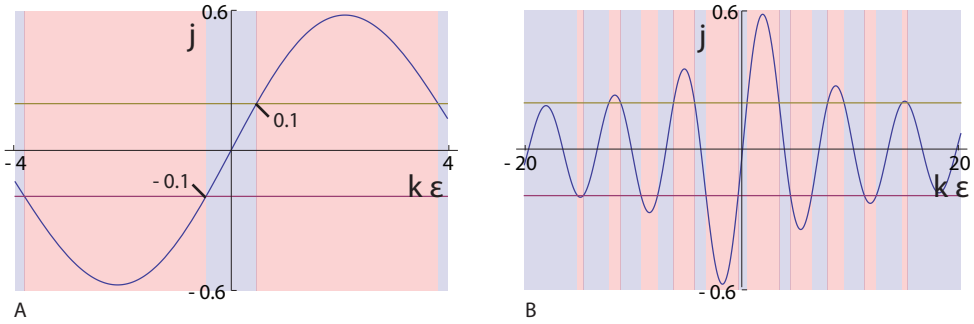

Figure 10.2: These figures mark the limits given by eqs. (10.4) and (10.5) in a graph of the Bessel function $J_1(k\epsilon)$. The blue shaded regions mark the trapping values for ϵ whereas the red areas mark the not trapping values for $k\epsilon$. In figure A the plot shows a small range ($-4 < 4\epsilon < 4$) of the Bessel function. It shows the first trapping region which is $|4\epsilon| < 0.41$. Figure B shows the full range over which all the anti-trapping regions our found. The yellow line is plotted at the maximum value $j = 1/5$ and the red line at the minimum value $j = -1/5$.

In figure 10.3 the number of atoms is shown as a function of the anisotropy ϵ. The plot shows that at $\epsilon = 0.10$ and $j \simeq 0.2$ the atoms are lost which is a logical consequence of the anti-trapping potential above $\epsilon = 0.1$ and $j \simeq 0.2$ for the Quadpod (see figure 10.2) at critical rotation. Another clear feature

is that from $\epsilon = 0.04$ and $j \simeq 0.08$ on the atom number is linearly decreasing. It is feasible that this is caused by the trap opening up and the cloud is getting so large that a great part of the atoms are evaporated away by the rf-shield. Also these measurements were done with only one phase of the TOP trap, so everything (evaporation and final thermalisation) was done in a rotating trap. We will need to further investigate these phenomena before we are able to make conclusive statements.

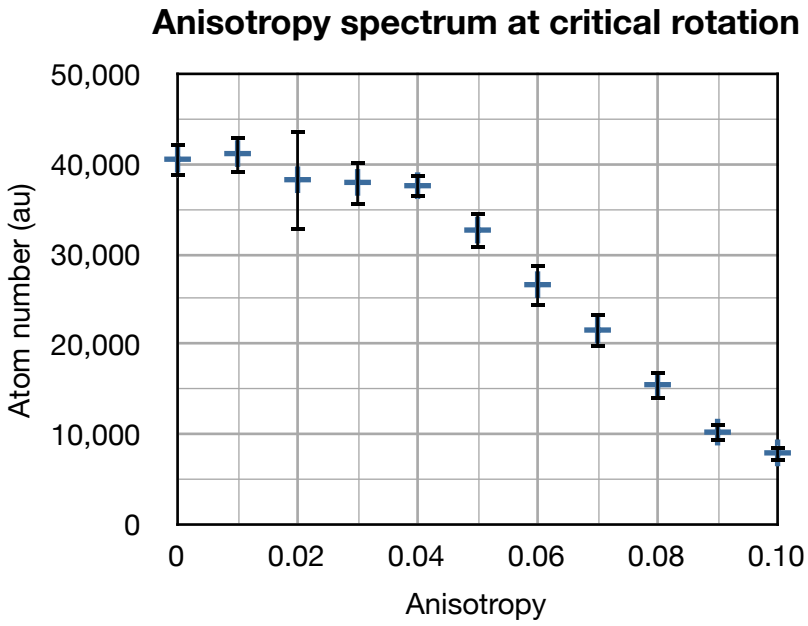

Figure 10.3: PRELIMINARY: Atom number as a function of the anisotropy. Shown is the fact that at $\epsilon = 0.1$ and $j \simeq 0.2$ the atom number is decreasing. Another feature is that from $\epsilon = 0.04$ and $j \simeq 0.08$ the atom number is decreasing, which might be caused by the trap lowering its barrier at critical rotation and "strong" anisotropy j. The points in the graph are an average of multiple measurements and the error bars are the standard errors of each points, calculated by $\sigma_{\text{se}} = \sqrt{\langle y - \langle y \rangle \rangle^2 / N^2}$, with N the number of points and $\langle y \rangle$ the average of y-values.

Conclusion and Summary

INTERESTING - We have shown that rotating an atom cloud using phase modulation of a TOP trap is an interesting system for studying ultra cold atoms in the co-rotating frame. Setting the shaped potentials created using phase modulation into rotation is done using a simple scheme and the potential in the co-rotating frame only changes due to the centrifugal potential.

Experimentally, the formalism is explored in both a rotating Dipod ($N = 2$) and Quadpod ($N = 4$). The first measurements provided use with a rotation spectrum of both the Dipod and Quadpod. These spectra show that around critical rotation the Dipod is anti-trapping whereas the Quadpod for a certain anisotropy strength can be trapping at the point of critical rotation.

With the second series of measurements we investigated the strength of the anisotropy at critical rotation of a Quadpod and compared the results with the analytical predictions for the trapping window of the Quadpod potential. The result and predictions seemed to be in perfect agreement, although it must be noted that the decrease of atom number before the threshold can not yet the explained quantitatively. More investigation is needed.

Also it need be noted that the experiments on anisotropy strength at critical rotation were done in the first run mode (discussed in subsection 2.2.1), which has the rotating shaped TOP trap during evaporation and decompressing of the TOP trap.

CHAPTER 10: RESULTS

Appendix

APPENDIX A

Integrating Jacobi-Anger expanded functions

JACOBI-ANGER EXPANSION was introduced to describe plane waves as a sum of cylindrical waves (Abramowitz & Stegun, 1972). In the following chapter we use this formalism to solve the integral of multiple angle phase modulated functions.

A.1 Jacobi-Anger expansion

The Jacobi-Anger expansion is based on a Laurent series for a generating function,

$$e^{(z/2)(t-1/t)} = \sum_{n\in\mathbb{Z}} J_n(z)t^n, \tag{A.1}$$

where $z \in \mathbb{C}$, t a generating function and J_n the n^{th} order Bessel function. The Jacobi-Anger expansion for a sine in the argument of an exponential function is generated by

$$\begin{aligned} t &= e^{i\phi} \\ e^{iz\sin\phi} &= \sum_{n\in\mathbb{Z}} J_n(z)e^{i\phi n} \end{aligned} \tag{A.2}$$

and finally the Jacobi-Anger expansion for sine phase modulation is obtained.

A.2 Jacobi-Anger expansion for phase modulated functions

Phase modulation can be described with a phase function $\Phi_{\text{sin}}(\tilde{t})$ inside a (co)sine, with $\tilde{t}$ the time normalised to the unit of one oscillation period,

$$\Phi_{\text{sin}}(\tilde{t}) = 2\pi\tilde{t} + \epsilon\sin(2\pi N\tilde{t}).$$

The phase modulated cosine is then expanded as

$$\cos\left(\Phi_{\text{sin}}(\tilde{t})\right) = \sum_{n\in\mathbb{Z}} J_n(\epsilon)\cos(2\pi\tilde{t}(Nn+1)) \tag{A.3}$$

and the sine as

$$\sin\left(\Phi_{\text{sin}}(\tilde{t})\right) = \sum_{n\in\mathbb{Z}} J_n(\epsilon)\sin(2\pi\tilde{t}(Nn+1)). \tag{A.4}$$

A.3 Multiple angle expansions

Multiple angle trigonometric functions are important for describing powers of trigonometric functions. Phase modulation can be described with a phase function $\Phi_{\text{sin}}(\tilde{t})$ inside a (co)sine, with $\tilde{t}$ the time normalised to one oscillation period. The $k \in \mathbb{N}$ is added to define the multiple angle. First the phase modulated cosine is given by

$$\cos\left(k\Phi_{\text{sin}}(\tilde{t})\right) = \sum_{n\in\mathbb{Z}} J_n(k\epsilon)\cos(2\pi\tilde{t}(Nn+k)) \tag{A.5}$$

and then the sine by

$$\sin\left(\Phi_{\text{sin}}(\tilde{t})\right) = \sum_{n\in\mathbb{Z}} J_n(k\epsilon)\sin(2\pi\tilde{t}(Nn+k)). \tag{A.6}$$

A.4 Integration of a multiple angle phase modulated functions

The last procedure is to integrate over one cycle period. First for a cosine:

$$\begin{aligned}\int_0^1 \cos(k\Phi_{\text{sin}}(\tilde{t}))d\tilde{t} &= \sum_{n\in\mathbb{Z}} J_n(k\epsilon)\int_0^1 \cos(2\pi(Nn+k))d\tilde{t} \\ &= \sum_{n\in\mathbb{Z}} J_n(k\epsilon)\delta_{Nn,k}.\end{aligned}$$

Then for a sine:

$$\begin{aligned}\int_0^1 \sin(k\Phi_{\sin}(\tilde{t}))d\tilde{t} &= \sum_{n\in\mathbb{Z}} J_n(k\epsilon)\int_0^1 \sin(2\pi(Nn+k))d\tilde{t}\\ &= 0,\end{aligned}$$

which provides the necessary tools to solve the expanded phase modulated TOP potentials (see Part II).

APPENDIX A: INTEGRATING JACOBI-ANGER EXPANDED FUNCTIONS

APPENDIX B

Properties of a 4^{th}-order potential

FOURTH-order potentials are of great interest in rotating systems, because they are the lowest trapping order when the harmonic potential is removed. We would like to know for which parameters $a, b \in \mathbb{R}$ the following 4^{th}-order potential has a local minimum in the centre:

$$f(x, y) = a(x^4 + y^4) + b\, x^2 y^2, \tag{B.1}$$

where x and y are the parameters in the plane. Next we calculate the gradient of the potential in the xy-plane and project this onto a arbitrary direction $\boldsymbol{r} = r\cos\theta\,\hat{\boldsymbol{x}} + r\sin\theta\,\hat{\boldsymbol{y}}$ with r the distance from the centre and θ the angle with respect to the positive x-axis,

$$\begin{aligned}
\boldsymbol{\nabla} f(x, y) &= 4\,a\left(x^3\hat{\boldsymbol{x}} + y^3\hat{\boldsymbol{y}}\right) + 2\,b\left(xy^2\hat{\boldsymbol{x}} + x^2 y\hat{\boldsymbol{y}}\right) \\
&= 4\,ar^3\left(\cos^3\theta\,\hat{\boldsymbol{x}} + \sin^3\theta\,\hat{\boldsymbol{y}}\right) + 2\,b\,r^3\left(\cos\theta\sin^2\theta\,\hat{\boldsymbol{x}} + \cos^2\theta\sin\theta\,\hat{\boldsymbol{y}}\right); \\
\boldsymbol{r}\cdot\boldsymbol{\nabla} f(x, y) &= 4\,r^4\left[a\left(\cos^4\theta + \sin^4\theta + 2\cos^2\theta\sin^2\theta\right) + (b - 2a)\cos^2\theta\sin^2\theta\right] \\
&= 4\,r^4\left[a + \frac{1}{4}(b - 2a)\left(\frac{1}{2} - \frac{1}{2}\cos 4\theta\right)\right].
\end{aligned}$$

A local minimum in the centre means that the gradient in all directions should be pointing outward. In this case we can make it even stronger and find the parameters for a global minimum there. This gives a strong condition on the projection of the gradient,

$$4\,r^4\left[a + \frac{1}{4}(b - 2a)\left(\frac{1}{2} - \frac{1}{2}\cos 4\theta\right)\right] > 0.$$

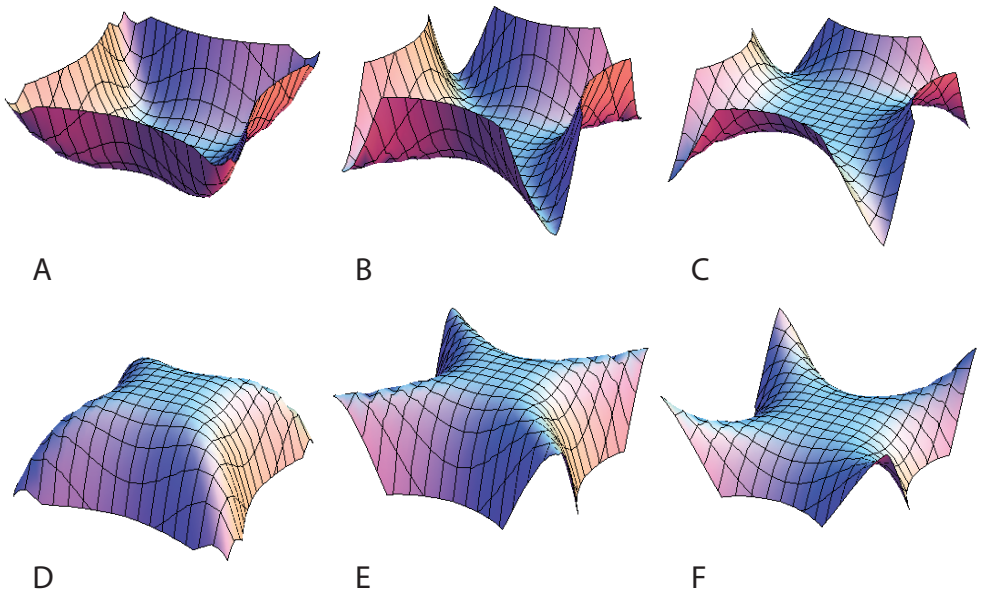

Figure B.1: The possible combinations of a and b are given by the six images. A. $a > 0 = 1$ and $b > -2a = -1.5$ which is trapping; B. $a > 0 = 1$ and $b = -2a = -2$ which is on the limit; C. $a > 0 = 1$ and $b < -2a = -2.5$ which is not-trapping; On the next row all the potentials are not-trapping because of $a < 0$; the different images plotted are for different b. D. $b < -2a = 1.5$; E. $b = -2a = 2$; F. $b > -2a = 2.5$. The images confirm what is derived in eqs. (B.3) and (B.4)

.

When looking for a local minimum the limit, $r \to 0$ needs be taken, but since $r > 0$ by definition, we find that it is equivalent for all r and thus we can find parameters for having a global minimum at the centre. Introducing $\alpha = \frac{1}{2} - \frac{1}{2}\cos 4\theta$ then it follows that $\forall\theta$: $0 \leq \alpha \leq 1$;

$$a + \frac{1}{4}(b - 2a)\alpha > 0. \tag{B.2}$$

The case that $\alpha = 0$ gives the limit:

$$a > 0. \tag{B.3}$$

Next for $\alpha \in \langle 0, 1]$ we can write

$$\begin{aligned} b &> -2a\frac{2-\alpha}{\alpha} = -2a\left(1 - \frac{2}{\alpha}\right) \\ &> -2a \qquad\qquad \forall\alpha \in \langle 0, 1]. \end{aligned} \tag{B.4}$$

To finalise a needs to be always positive and the limit of b is defined by a as $b > -2a$. In figure B.1 six different situations are plotted. And clearly only the first one with $a > 0$ and $b > -2a$ is trapping.

Appendix B: Properties of a 4TH-order potential

APPENDIX C

Cicero Word Generator

EXPERIMENTAL CONTROL - Every experiment relies on computers to synchronise different steps in the experiment. The computer itself uses software to create the right order of steps (a sequence). From the beginning of the experiment on a home build program was used, which had to be reprogrammed when a new time step or device was added. This costed a lot of valuable time that could be used better. The solution was to use a program which was already used by the neighbouring lab: Cicero Word Generator (Keshet, 2008).

Cicero Word Generator is split up in three parts. The first part is Atticus which is the 'server' application that runs on the computer that runs the experiment. The second is Cicero which is the 'client' application and graphical interface to the program. With Cicero several 'servers' can be controlled and provided with instructions. The third part is called Elgin and is only used to read log files. From now on we will only discuss Atticus and Cicero, because these are the most important for the experiment.

In this chapter we will discuss the features added to make Cicero work with the experiment. In Code example like C.1, C.2, C.4, and C.5 we have used the definition that $(\dots)$ means a variable defined by the script around the given code, $[\dots]$ a variable defined in the $\langle Variables(F7)\rangle$-tab and $<\cdots>$ as variables given by the HardwareSettings.

C.1 Tabor WW1072: Programming Standard TOP

Programming of a Standard TOP trap requires to send two unmodulated sinusoidal function, with 90° phase difference between the two signals, to the two coil pairs. Cicero supports sending GPIB parameter lists to any GPIB device this can be done in the tab $\langle$GPIB (F4)$\rangle$. Where a new GPIB

group was created and the channel of the Tabor WW1072 was enabled. When the channel is enabled one can chose the GPIB mode **Parameter** from a drop-down menu and then the following parameters were used.

Listing C.1: GPIB code: Standard TOP

```
// Set the device to the GATED mode
:INIT:CONT 0
:TRIG:GATE 1
:TRIG:BURS 0
:TRIG:SOUR:ADV EXT
:TRIG:PHAS 0
:TRIG:SLOP POS
:FUNC:MODE FIX
:FREQ [TOPnu]
:OUTP:SYNC:STAT 0
// Set channel 1 to output a cosine signal
:INST:SEL 1
:FUNC:SHAP SIN
:SIN:PHAS 90
:VOLT 3.375
:AM 1
:OUTP 1
// Set channel 2 to output a sine signal
:INST:SEL 2
:FUNC:SHAP SIN
:SIN:PHAS 180
:VOLT 3.375
:AM 1
:OUTP 1
```

The first part was used to set the Trigger mode to **Gated** such that a digital channel can be used to define the periods during which the TOP needs to be on. It also defines the frequency [TOPnu] based on an Cicero interface variable for outputting a **Fixed** function.

The second part defines the output for channel one and gives it a sine with amplitude 3.375 volt and turns amplitude modulation and the outputting on.

The third part does the same as the second part, but this time for channel two and with a 90° phase difference.

To execute a TOP trap the only thing that needs to be done is making a **Sequence** in Cicero and setting the GPIB group made for the TOP trap

to an early segment[1]. The next step is to add a digital trigger that gates the signal send from the Tabor device.

C.2 Magnetic Transport

The magnetic transport is in detail explained in the thesis of Marc Cheneau (Cheneau, 2009), we only needed to implement the use of the magnetic transport in Cicero. The magnetic transport is powered by a number of power supplies and the currents that these supplies output is controllable with analog channels. In Cicero this can be done using the ⟨Analog (F3)⟩-tab and making several groups that corresponds to the different phases in the transport. All that needed be done was writing a script (in Python) for converting the current files which give the currents through the coil pairs as a function of the position of the cloud. The package is called **Transport Currents** and contains all the necessary files to create different transport possibilities. The package has an extensive *README* which guides through the process of creating files that can be imported into Cicero.

C.3 Agilent N5181: Programming Evaporation Ramp

For evaporation we use the Agilent N5181, because it has the ability to program a point list (up to 1600 points) with frequency and amplitude values and output a function that is based on these properties when a triggering signal is send. Originally Cicero did not have the feature to first send the data en then trigger with a digital signal. To overcome this lack of functionality we have implemented the A+F trig mode for GPIB and the Agilent N5181 in specific. The idea of this mode is to set the device such that it takes a point list and wait for a trigger.

In Listing C.2 a snippet of GPIB code send to the Agilent is shown and we are going to explain some of it: Line 2 is to set the unit of Power to the device, this can be set in the HardwareSettings for the specific device under **GPIB**. Line 3 through 5 are used to set the type of outputting to a List of point given in Lines 7 and 8. Line 6 sets whether after a full output the device should go back to the first point in the list (this can be set in the HardwareSettings under **GPIB**). Line 9 and 10 set the change to the next

[1]This segment needs to at least last 100 ms before the triggering signal is given, because the sending of the GPIB data needs to be finished before triggering. Usually a good place to send the data is during the MOT phase

point to be based on an internal timer with the variable *secondsPerSample* that gives the time in between two point. Line 11 and 12 set the trigger to an external input and finally the output is turned on after a trigger.

Listing C.2: GPIB code: Evaporation with mode **A+F trig**

```
1  // Set the device for frequency and amplitude
2  // modulation using a point list
3  :LIST:TYPE:LIST:INITialize:PRESet
4  :UNIT:POWer <amplitudeUnit>
5  :SOURce:FREQuency:MODE LIST
6  :SOURce:POWer:MODE LIST
7  :SOURce:LIST:TYPE LIST
8  :SOURce:LIST:RETRace <Retrace>
9  :SOURce:LIST:POWer (amplitudeList)
10 :SOURce:LIST:FREQuency (frequencyList)
11 :SOURce:LIST:TRIGger:SOURce TIMer
12 :TRIGger:SEQuence:TIMer (secondsPerSample)
13 :TRIGger:SEQuence:SOURce EXT
14 :INITiate
15 :OUTput:STATe ON
```

C.4 Converting Interface Unit to Voltages

The analog channels of the outputting cards can only output voltages from 0 to 10 V, but with these voltages other devices are controlled that themselves control other quantities then voltage. In the interface we needed an conversion, such that these other quantities with their respective units could be used in the interface, but the outputting is still done in voltages.

To accomplish this we added converter code to Atticus and a conversion interface to Cicero. The conversion interface can be found in the **Channel Manager** window, where two columns have been added: *Unit* and *Conversion*. The possible units are: s (seconds); V (Voltage, standard), Hz (Hertz), A (Amperes), deg (Degrees), dBm (decibel milli Watt) and Pr (percentage). Extra units can be added by modifying the file **Units.cs** in project **DataStructures**. The column *Conversion* should have a valid **dotMath** equation with the name of the unit used as a variable. For example standard *Unit* is set to **V** and the equation would then standard be **V**, but another possible equation would be: **1+2*V**. More information about equations can be found in the documentation of Cicero (Keshet, 2008).

Atticus uses the *Unit* and *Conversion* values to transform analog data points, for a certain logical channel, into voltages. This conversion is done in the file **DaqMxTaskGenerator.cs** at three places. This is needed because of the structure of Atticus which consists of a part that handles the ⟨Output Now⟩ mode, and two parts that handle the *Sequenced* mode, one with and one without *Variable Timebase*. The conversion is done with the following function that takes *double* **bufferValue** as the input value and using *dotMath.EqCompiler* **eq** and *Units.Dimension* **unit** to convert a value in interface units to a voltage.

Listing C.3: Function to convert a interface unit to a voltage

```
1  public static double convertDimensions(
2     double bufferValue,
3     dotMath.EqCompiler eq,
4     Units.Dimension unit)
5  {
6     double convertedValue = 0;
7     // Give the value of the variable
8     eq.SetVariable(unit.ToString(), bufferValue);
9     try
10    {
11       double val = eq.Calculate();
12       if ((!double.IsInfinity(val)) &&
13          (!double.IsNaN(val)))
14       {
15          convertedValue = eq.Calculate();
16       }
17    }
18    catch (Exception e) { }
19    return convertedValue;
20 }
```

After these conversions new data lists are created and send to the buffers of analog outputting cards.

C.5 Variable Timebase

To improve the time resolution possible in our experiment we have implemented the **Variable Timebase** mode in Cicero based on the instructions in (Keshet, 2008). To make this possible a new PXI was installed: the PXI-6534

from National Instruments. This card now operates on a high resolution and makes sure that the other cards only change their outputting when something is changed. The big advantage is that during a MOT phase now the analog channels do not need to constantly output and this drastically reduce the memory used and thus we can improve the resolution.

C.6 Tabor WW1072: Programming Phase Modulated TOP

In section 2.2.1 we already explained the two different modes used in the experiments described by this thesis. In this section we will give some more detail on the difference between the two modes.

C.6.1 Gated mode

The first is best described as being the **Gated** mode. This means that only one type of waveform is defined and it is outputted by the Tabor WW1072 during a high signal of its trigger input - *Gated triggering*. In Listing C.4 the GPIB code that is send to the Tabor is shown. Lines 2 - 6 define the *Gated trigger* mode. Line 7 gives the phase offset between the two channels and Line 8 sets the frequency (*outputtingFrequency*) at which the individual data points of the waveform need be outputted. The variable (*outputtingFrequency*) is calculated taking the number of points in a single waveform η and multiplies this with the frequency at which the full waveform needs to be outputted $[TOPnu]$.

The second part defines the waveform data points for each channel and sends these to the device. Line 11 - 13 sets the channel, its amplitude and that it can be modulated using an external analog signal. Line 14 - 18 loads the waveform data to the device. Where (*numberPoints*) is $\eta \cdot p$ and (*buffer*) is $2\,\eta \cdot p$ (each point used two times four bits) and (*bufferLength*) is the length of the string (*buffer*) in ASCI characters. (*waveformData*) is the actual data in binary form to speed up the transfer. Finally, Line 19 set the channel to output when a high signal (*Gated trigger*) is received.

Listing C.4: GPIB code: TOP with mode **Gated**

```
1 // Set the GATED mode
2 :FUNC:MODE USER
3 :INIT:CONT 0
4 :TRIG:GATE 1
```

```
5  :TRIG:BURS 0
6  :TRIG:SOUR:ADV EXT
7  :PHAS:OFFS 0
8  :FREQ:RAST (outputtingFrequency)
9  // This is repeated for the number of channels on
10 // the device (in our case 2)
11 :INST:SEL (channelNumber)
12 :VOLT (channelAmplitude)
13 :AM 1
14 :TRAC:DEF 1,(numberPoints);:TRAC:SEL 1
15 *CLS
16 *CLS;*OPT;:TRAC:DATA #(bufferLength)(buffer)
17 (waveformData)
18 *CLS
19 :INST:SEL (channelNumber);:OUTP 1
```

C.6.2 Segmented Mode

The second mode is based on the first, but instead of have one waveform and outputting that during a high signal on the *Trigger in* port. This mode can accommodate several waveforms and switch between these when a rising slope is send to the *Trigger in* port. In Listing C.5 the GPIB commands are shown that are send to the Tabor WW1072 to initialise the **Segmented** mode and to end the waveform data. Lines 2 - 8 are the same as in the **Gated** mode. The same holds for lines 14 - 20 and 24 - 30.

The big differences are Line 21 and Line 31 which define at which point in the sequence a segment has to come. Line 21 does that for the constant amplitude phase (which is needed because it is not possible to trigger the first segment. In stead the constant phase in outputted after the sending of the data and a trigger is send when the first waveform needs to be send).

Line 31 set the position of segment defined by Lines 24 - 31. This part of the code loops over the different available segments with ID (*segmentNumber*).

Finally, the last part Line 34 and 35 are looped over the available channels. Line 34 sets all channels to have amplitude modulation and Line 35 makes all the channels turn their output on.

Listing C.5: GPIB code: TOP with mode **Segmented**

```
1 // Set the SEGMENTED mode
2 :FUNC:MODE USER
3 :INIT:CONT 1
```

```
:TRIG:GATE 0
:TRIG:BURS 0
:TRIG:SOUR:ADV EXT
:PHAS:OFFS 0
:SEQuence:DELete:ALL
:TRACe:DELete:ALL
:SEQuence:ADVance STEP
:FREQ:RAST (outputtingFrequency)
// This is done to given an initial constant signal
// to both channels
:INST:SEL (channelNumber)
:VOLT (channelAmplitude)
:TRAC:DEF 1,(numberPoints);:TRAC:SEL 1
*CLS
*CLS;*OPT;:TRAC:DATA #(bufferLength)(buffer)
(waveformData)
*CLS
:SEQuence:DEFine 1,1,1,1
// This is looped over the number of channel and the
// number of needed segments
:INST:SEL (channelNumber)
:VOLT (channelAmplitude)
:TRAC:DEF (segmentNumber),(numberPoints);:TRAC:SEL (
   segmentNumber)
*CLS
*CLS;*OPT;:TRAC:DATA #(bufferLength)(buffer)
(waveformData)
*CLS
:SEQuence:DEFine (segmentNumber),(segmentNumber),1,1
// This is looped over the number channel to set
// them all to outputting
:INST:SEL (channelNumber);:AM 1
:INST:SEL (channelNumber);:OUTP 1
```

Epilog

Perspectives

RESEARCH answers a lot of questions, but often an answered question poses multiple new questions. The same is true for this research, because the question whether we can use phase modulation as a technique for making rotating systems seems to be answered with a yes, but the research has brought us with a lot of questions. A good example is whether it is possible to reach the regime of strongly correlated systems, but even closer to the research done in this report one can ask himself why the atoms react so strongly on very strong phase modulation. To answer these questions a lot of further investigation is needed.

That is also the reason for the group to continue with what we have started. The first thing that is done a the moment of writing is installing new imaging equipment for more qualitative measurements. The next step will be doing the same experiments as before and trying to see vortices in the Quadpod at critical rotation.

Another interesting, and yet not understood feature, is found in sections 4.2 and 7.2. Where there is some evidence that, if the rotation of the bias field changes to rapidly the atoms are strongly influenced. Investigating this hypothesis might be done with simulations that keep track of the internal degree of freedom (no adiabatic approximation), while evolving two (for spin 1/2 particles) or three (for spin 1 particle) coupled time-dependent Schrödinger equations.

In the far future geometrical potentials (Günter, Cheneau, Yefsah, Rath, & Dalibard, 2009) and 2D systems provide the group with interesting phenomena to study. Finally, the goal is to reach the strongly correlated regime either with rotation or these geometrical potentials and whether that is feasible or not needs to be investigated.

APPENDIX C: PERSPECTIVES

Acknowledgments

ONE year is a long time, but this year in Paris seemed to have flown by. The reason for that is the partly the place where this research was done. First the team in which I did my work. Tarik (I still want to see that 4-0, for the Netherlands of course), Rémi, Laura, Laurianne, Patrick and Ken (Dude, dude, dude, ohw, no nothing!). But also the great guide during this period, Jean Dalibard, who seemed to be able to give me the right direction when I though I was completely stuck. Secondly the people from the other groups: Sebastian (Sebi), Franz(el) (I like the slacklining), Julliette, Sanjukta, Jerom, Luigi (thanks for the soldering tips), Emmanuel (incredible patience with me and Cicero), David, Fabrice, Nir, Sylvain, Ulrich, Armin, Thomas, Frédérick and Christophe.

I would like to thank Gora for inviting me to have a look in Paris *en Jook voor het goede advies dat hij mij op bepaalde momenten graag wilde geven, maar ook Robert voor het zijn van mijn supervisor.*

The other part was done by the friends I have made here: Petra, Jeanrique, Artem, Kamil, Werner, Jasper, Marco, Rafaël, Hanne, Dion, Bouke, Sam, Nienke, Nynke, Lennert, Neuza, Yvonne, Leonor, Lorijn, Marina, Zosia, Mark, Mieke, Pol, Annabel, Carlo. And above all of course: Jan-Phillip *voetbal zal nooit hetzelfde meer zijn*, Joana Bazingaaaaaah!, Samuele Watch-out don't laugh too much.

Nathalie en Jeroen bedankt voor de steun die ik heb gehad in de periode voor dat ik naar Parijs ging. En Carola ik wens je heel veel sterkte toe in de tijd die gaat komen en ik wil jou ook bedanken voor alles wat je voor mij hebt gedaan. Jeroen wil ik bedanken voor het luisterende oor die hij mij kon geven, maar ook de afleiding in Artis. Er zijn mensen die ik graag wil bedanken voor het feit dat ze langs zijn gekomen of door mijn stomheid niet konden en voor het 'gewoon' een vriend zijn, Kasper en Bart super bedankt voor de super gave tijd. Ik wil Floor bedanken voor het feit dat hij een vriend is die met één woord weet wat er door mij heen gaat en gewoon zegt waar het op staat.

Appendix C: Acknowledgments

Ik wild tante T. bedanken dat ze mij zoveel steun heeft gegeven door hele veel kleine, maar ook grote, dingen te doen die het weg zijn makkelijker hebben gemaakt.

Ik wil mijn ouders bedanken voor hun steun tijdens al die jaren van school en studie, maar ook tijdens de periode voordat ik wegging die gewoon heel zwaar is geweest. Daarnaast weet ik dat mijn moeder het heel erg moeilijk heeft gehad dat ik voor een jaar weg ben geweest en dat daar nu een nog langere tijd, dat ik weg ben, aan zit te komen. Mam, Pap bedankt!

And jij sußig, merci.

Critical Rotation

Generally accepted there are three regimes of rotation which characterised by the number of atoms per vortex ν. The first one is the regime of slow rotation with $\nu \simeq 10^5$ this is on the order of one vortex in a condensate. The second regime is called the mean-field regime and is given by $\nu \simeq 10^3$. Finally, the third regime is characterised by $\nu \simeq 10^1$ and is called the strongly correlated regime. The third regime is of great interest for physicists, because the strongly correlated regime is not well understand theoretically and might explain (Fractional) Quantum Hall physics.

The third regime is reached by increasing the size of the condensate, reducing the number of atoms and increasing the rotation frequency. In our experiment we use the centrifugal force to fully compensate for the harmonic trapping potential and make the cloud as large as possible using the fourth order potential. This is called critical rotation.

In this report we use the Time-average Orbiting Potential (TOP) trap which is a trap made of a quadrupole trap together with a rotating bias field and modulate the rotation speed of this bias field. With this technique we are able to produce versatile potentials with all possible geometries.

The first step in producing these versatile potentials is trying to get the strongest anisotropies possible by choosing the geometry $\eta = 1, 2, \ldots$ and dividing that number points equally over a circle. The next step is to let the quadrupole field zero magnetic field point jump from one point to the other. This will give the strongest anisotropy for symmetry η. This turned out not to be a big success, because it strongly influenced the atoms and it turned out that $\eta = 64$ was most favourable for the atom number.

The next step is to take these $\eta = 64$ points and spread them out over the circle. This time not equally divide, but grouped in $N = 1, 2, \ldots$ groups with phase modulation. How strongly these points are grouped determines the strength of the anisotropy and now N is the symmetry. We have been looking at number of atoms as a function of the strength of the anisotropy and some interesting behaviour was found. $N = 2$ (Dipod) and $N = 4$

(Quadpod) showed a linear decreasing behaviour whereas the $N = 3$ (Tripod) shows a plateau with a threshold above which all the atoms are lost.

Finally, these phase modulated potentials are set into rotation and we have been looking at the rotation spectra of the three symmetries as well as the strength of the anisotropy at critical rotation for a Quadpod. The rotation spectra show the expected behaviour of a Dipod losing all the atoms at critical rotation due to the dynamical instability and the Quadpod showing that it stays trapping at critical rotation. We have also shown that this behaviour is to be expected from analytical calculations.

The strength of the anisotropy for a Quadpod at critical rotation lets itself explain partially, we can explain the moment where all the atoms are lost, but the point where the atoms start to be lost still needs to be investigated.

So far the results are promising for rotating condensates at the point of critical rotation.

Kritische rotatie

SINDS in de jaren '90 de groepen van *Cornell* en *Ketterle* (Anderson et al., 1995; Davis et al., 1995) onafhankelijk voor de eerste maal een Bose-Einsteincondensaat (BEC) wisten te produceren zijn wetenschappers bezig geweest met het bestuderen van dit fenomeen. Een BEC wordt gekarakteriseerd door de eigenschap dat het condensaat volledig fase coherent is. Dit heeft tot gevolg dat het condensaat een snelheidspotentiaal bezit wat op zichzelf weer de rede is voor het feit dat een condensaat geen rotatie kan bevatten.

Dit feit is heel merkwaardig en het heeft wetenschappers lange tijd doen verbazen. Tot in 1955 Feynman (Feynman, 1955) ontdekte dat het condensaat plaatsen kan creëren waar de fase ongedefinieerd is en de dichtheid van het condensaat naar nul gaat. Deze plaatsen worden draaikolken genoemd en bevatten de rotatie van het condensaat.

De rotatie van het systeem kan ingedeeld worden in drie categorieën op basis van het aantal atomen per draaikolk ν: De eerste categorie is langzame rotatie en dan gaat het over één draaikolk in het condensaat met $\nu \simeq 10^5$; de tweede categorie is de 'mean field' categorie met $\nu \simeq 10^3$ en heel veel draaikolken in een wolk; De laatste categorie is de sterk wisselwerkende categorie waarbij het aantal atomen overeenkomt met het aantal draaikolken $\nu \simeq 10$. Deze laatste categorie is interessant voor wetenschappers, omdat dit veel onverklaarde fysica herbergt en ook veel overeenkomst vertoont met magnetische systemen.

Het aantal atomen per draaikolk kan worden verkleint door of het oppervlakte van de wolk te verkleinen, of het aantal atomen te verminderen, of de rotatie snelheid op te voeren. In ons geval is gekozen om het oppervlakte zo groot mogelijk te maken en al het andere onveranderd te laten. Dit omdat we aan de éné kant worden gelimiteerd door onze afbeeld apparatuur en aan de andere kant is de val die wij gebruiken gelimiteerd in hoe snel het een wolk kan laten roteren.

Wij maken gebruik van een Time-averaged Orbiting Potential (TOP)

val. Deze val bestaat uit een kwadrupel val waarvan het nul punt, in het magnetische veld, om de wolk heen wordt geroteerd. Door de snelheid van deze rotatie te veranderen kunnen wij de vorm van de potentiaal aanpassen en deze vorm op zijn beurt weer roteren.

De eerste experimenten die hiermee gedaan zijn is het definiëren van $\eta = 1, 2, \ldots$ punten op een cirkel en het nul punt van de kwadrupel val van punt naar punt laten springen. Uit deze experimenten bleek dat de atomen hier sterk op reageren en dat minimaal $\eta = 64$ punten gedefiniërd moeten zijn. Om dus een sterke vorm te krijgen kunnen we niet het aantal punten verminderen.

De volgende stap is om $\eta = 64$ aan te houden en deze punten te verspreiden over de cirkel. Dit keer niet gelijk verdeelt, maar gegroepeerd gebruikmakend van fase modulatie. De vorm wordt nu bepaald door het aantal groepen $N = 1, 2, \ldots$ van punten en de sterkte van de vorm ϵ door hoe sterk ze zijn gegroepeerd. Vervolgens hebben wij gekeken naar het effect van de sterkte op het aantal atomen en wat bleek is dat voor $N = 2$ (Dipod) en $N = 4$ (Quadpod) er een lineair verval te zien was in tegenstelling tot $N = 3$ (Tripod) die een plateau laat zien tot op zekere hoogte een drempel is bereikt.

De laatste experimenten zijn gedaan aan het laten ronddraaien van de eerder genoemde vormen $N = 2$ en $N = 4$ en dan te kijken naar het aantal atomen als een functie van de rotatie snelheid. Dit geeft het rotatie spectrum voor de Dipod welke duidelijk laat zien dat er bij kritische rotatie geen atomen gevangen blijven. In tegenstelling tot de Quadpod die wel atomen gevangen houdt bij kritische rotatie. Vervolgens is er gekeken naar de sterke van de vorm bij kritische rotatie van een Quadpod. Wat blijkt is dat voorspeld kan worden dat bij een zekere sterkte geen atomen gevangen meer blijven en dit ook overeenkomt met het experiment.

Er zijn wel nog vele vragen die onbeantwoord blijven bij deze experimenten dus dit vereist nog verder onderzoek.

References

Abramowitz, M., & Stegun, I. (1972). *Handbook of mathematical functions with formulas, graphs, and mathematical tables*. 978-0-486-61272: Dover Publications.

Anderson, M. H., Ensher, J. R., Matthews, M. R., Wieman, C. E., & Cornell, E. A. (1995). Observation of Bose-Einstein Condensation in a Dilute Atomic Vapor. *Science*, *269*(5221), 198-201. Available from http://www.sciencemag.org/cgi/content/abstract/269/5221/198

Arlt, J., Maragò, O., Hodby, E., Hopkins, S. A., Hechenblaikner, G., Webster, S., et al. (1999). Bose-einstein condensation in a rotating anisotropic top trap. *Journal of Physics B: Atomic, Molecular and Optical Physics*, *32*(24), 5861. Available from http://stacks.iop.org/0953-4075/32/i=24/a=320

Barrett, M. D., Sauer, J. A., & Chapman, M. S. (2001, 06 19). All-optical formation of an atomic bose-einstein condensate. *Physical Review Letters*, *87*(1). Available from http://link.aps.org/doi/10.1103/PhysRevLett.87.010404

Bretin, V., Stock, S., Seurin, Y., & Dalibard, J. (2004, 02 04). Fast rotation of a bose-einstein condensate. *Physical Review Letters*, *92*(5). Available from http://link.aps.org/doi/10.1103/PhysRevLett.92.050403

Brink, D. M., & Sukumar, C. V. (2006, Sep). Majorana spin-flip transitions in a magnetic trap. *Physical Review A*, *74*(3), 035401+. Available from http://dx.doi.org/10.1103/PhysRevA.74.035401

Cheneau, M. (2009). *Transition superfluide et potentiels géométriques dans le gaz de bose bidimensionel*. Unpublished doctoral dissertation, ENS, Paris.

Cohen-Tannoudji, C., Diu, B., & Laloë, F. (1977). *Quantum mechanics* (Vol. 1). John Wiley and Sons.

Cooper, N. R., Wilkin, N. K., & Gunn, J. M. F. (2001, 08 30). Quantum phases of vortices in rotating bose-einstein condensates. *Physical Re-*

view Letters, *87*(12). Available from http://link.aps.org/doi/10.1103/PhysRevLett.87.120405

Davis, K. B., Mewes, M. O., Andrews, M. R., Druten, N. J. van, Durfee, D. S., Kurn, D. M., et al. (1995, Nov 27). Bose-einstein condensation in a gas of sodium atoms. *Physical Review Letters*, *75*(22), 3969–3973. Available from http://dx.doi.org/10.1103/PhysRevLett.75.3969

Feynman, R. P. (1955). *Progress in low temperature physics*. North Holland, Amsterdam.

Franzosi, R., Zambon, B., & Arimondo, E. (2004, Nov). Nonadiabatic effects in the dynamics of atoms confined in a cylindric time-orbiting-potential magnetic trap. *Phys. Rev. A*, *70*(5), 053603.

Gemelke, N., Sarajlic, E., & Chu, S. (2010). Rotating Few-body Atomic Systems in the Fractional Quantum Hall Regime. *ArXiv e-prints*.

Greiner, M., Bloch, I., Hänsch, T. W., & Esslinger, T. (2001, Feb). Magnetic transport of trapped cold atoms over a large distance. *Physical Review A*, *63*(3), 031401+. Available from http://dx.doi.org/10.1103/PhysRevA.63.031401

Guery-Odelin, D. (2000, 08 14). Spinning up and down a boltzmann gas. *Physical Review A*, *62*(3). Available from http://link.aps.org/doi/10.1103/PhysRevA.62.033607

Günter, K. J., Cheneau, M., Yefsah, T., Rath, S. P., & Dalibard, J. (2009, Jan). Practical scheme for a light-induced gauge field in an atomic bose gas. *Phys. Rev. A*, *79*(1), 011604.

Hodby, E., Hechenblaikner, G., Hopkins, S. A., Maragò, O. M., & Foot, C. J. (2001, Dec). Vortex nucleation in bose-einstein condensates in an oblate, purely magnetic potential. *Phys. Rev. Lett.*, *88*(1), 010405.

Keshet, A. (2008, June). Cicero word generator technical and user manual [Computer software manual].

Ketterle, W., & Druten, N. J. van. (1996). Evaporative cooling of trapped atoms. *Advances in Atomic, Molecular, and Optical Physics*, *37*, 56.

Landau, L. D., & Liftshitz, E. M. (1977). *Quantum mechanics: Non-relativistic theory* (3rd ed., Vol. 3). Pergamon Press.

Laughlin, R. B. (1999, 07 1). Nobel lecture: Fractional quantization. *Reviews of Modern Physics*, *71*(4). Available from http://link.aps.org/doi/10.1103/RevModPhys.71.863

Mewes, M. O., Andrews, M. R., Druten, N. J. van, Kurn, D. M., Durfee, D. S., & Ketterle, W. (1996, 07 15). Bose-einstein condensation in a tightly confining dc magnetic trap. *Physical Review Letters*, *77*(3). Available from http://link.aps.org/doi/10.1103/PhysRevLett.77.416

Minogin, V. G., Richmond, J. A., & Opat, G. I. (1998, 10 1). Time-orbiting-potential quadrupole magnetic trap for cold atoms. *Physical Review A*, *58*(4). Available from http://link.aps.org/doi/10.1103/PhysRevA.58.3138

Petrich, W., Anderson, M. H., Ensher, J. R., & Cornell, E. A. (1995, Apr 24). Stable, tightly confining magnetic trap for evaporative cooling of neutral atoms. *Physical Review Letters*, *74*(17), 3352–3355. Available from http://dx.doi.org/10.1103/PhysRevLett.74.3352

Pitaevskii, L., & Stringari, S. (2003). *Bose-einstein condensation*. Clarendon Press - Oxford.

Raab, E. L., Prentiss, M., Cable, A., Chu, S., & Pritchard, D. E. (1987, December). Trapping of neutral sodium atoms with radiation pressure. *Physical Review Letters*, *59*(23), 4.

Rath, S. P. (2010). *Production and investigation of quasi-two-dimensional bose gases*. Unpublished doctoral dissertation, L'Université Pierre et Marie Curie.

Rosenbusch, P., Petrov, D. S., Sinha, S., Chevy, F., Bretin, V., Castin, Y., et al. (2002, 06 07). Critical rotation of a harmonically trapped bose gas. *Physical Review Letters*, *88*(25). Available from http://link.aps.org/doi/10.1103/PhysRevLett.88.250403

Stormer, H. L., Tsui, D. C., & Gossard, A. C. (1999, 03 1). The fractional quantum hall effect. *Reviews of Modern Physics*, *71*(2). Available from http://link.aps.org/doi/10.1103/RevModPhys.71.S298

Tabor Electronics. (2005). Models 1071/1072 100 ms/s single / dual arbitrary waveform generators [Computer software manual].

Townsend, C. G., Edwards, N. H., Cooper, C. J., Zetie, K. P., Foot, C. J., Steane, A. M., et al. (1995, 08 1). Phase-space density in the magneto-optical trap. *Physical Review A*, *52*(2). Available from http://link.aps.org/doi/10.1103/PhysRevA.52.1423

References

Index